TFK1, a basal body transition fibre protein that is essential for cytokinesis in *Trypanosoma brucei*

Miharisoa Rijatiana Ramanantsalama[1], Nicolas Landrein[1], Elina Casas[1], Bénédicte Salin[2], Corinne Blancard[2], Mélanie Bonhivers[1], Derrick R. Robinson[1], Denis Dacheux[1,3]*

[1]University of Bordeaux, CNRS, Microbiologie Fondamentale et Pathogénicité, UMR 5234, F-33000 Bordeaux, France.

[2]University of Bordeaux, CNRS, Microscopy Department IBGC, UMR 5095, F-33000 Bordeaux, France

[3]Bordeaux INP, Microbiologie Fondamentale et Pathogénicité, UMR 5234, F-33000 Bordeaux, France.

*Author for correspondence

Corresponding author: Denis Dacheux

email: ddacheux@bordeaux-inp.fr

Address: University of Bordeaux, Microbiologie Fondamentale et Pathogénicité, UMR 5234, F-33000 Bordeaux, France

Tel: +33 (0)5 57 57 57 57; Fax: +33 (0)5 57 57 48 03.

Key Words

Trypanosoma brucei, transition fibres, Transition Fibres protein Kinetoplastid specific-1, TFK1, cytokinesis, basal body, flagellum, kinetoplastid, cytoskeleton.

Abstract

In *Trypanosoma brucei,* transition fibres (TF) form a nine-bladed pattern-like structure connecting the base of the flagellum to the flagellar pocket membrane. Despite the characterization of two TF proteins, CEP164C and *Tb*RP2, little is known about the organization of these fibres. Here, we report the identification and characterization of the first kinetoplastid-specific TF protein named TFK1 (Tb927.6.1180). Bioinformatics and functional domain analysis identified three TFK1 distinct domains: an N-terminal domain of an unpredicted function, a coiled-coil domain involved in TFK1-TFK1 interaction and a C-terminal intrinsically disordered region potentially involved in protein interaction. Cellular immuno-localization showed that TFK1 is a newly identified basal body maturation marker. Further, using ultrastructure expansion and immuno-electron microscopies we localized CEP164C and TbRP2 at the TF and TFK1 on the distal appendage matrix of the TF. Importantly, RNAi knockdown of TFK1 in bloodstream form cells induced misplacement of basal bodies, a defect in the furrow or fold generation and eventually cell death. We hypothesize that TFK1 is a basal body positioning specific actor and a key regulator of cytokinesis in the bloodstream form *Trypanosoma brucei*.

Introduction

Trypanosoma brucei (*T. brucei*) is a unicellular flagellated African protozoan parasite responsible for Human African Trypanosomiasis or « sleeping sickness » and nagana in livestock (Auty et al., 2015; Büscher et al., 2017; Steverding, 2008). *T. brucei* has complex life and cell cycles during transmission from the tsetse fly vector to the mammalian host with significant morphogenetic changes (Gull, 1999; Matthews, 1999). Among the different forms are the procyclic insect forms (PCF) in the insect midgut and the infectious bloodstream forms (BSF) upon transmission to the vertebrate host.

In both forms, a single flagellum nucleates from the basal body near the posterior end of the cell, exits the cell body through the flagellar pocket (FP), the only site for endo/exocytosis, and extends along the length of the cell toward the anterior end (Field and Carrington, 2009; Lacomble et al., 2009; Lacomble et al., 2010; Overath and Engstler, 2004). The cytoskeleton region between the basal bodies and the site where the flagellum exits the cell is quite complex. The basal bodies (BBs) are connected to the mitochondrial genome (kinetoplast) through the tripartite attachment complex (TAC) but also with the FP membrane through the transition fibres (TFs) (Ogbadoyi et al., 2003; Vaughan and Gull, 2016). The TF consist of a set of nine structures that are located on the mature basal body and radiate from the triplet of microtubules to connect it to the FP membrane (Geimer and Melkonian, 2004; Gonçalves and Pelletier, 2017; Lacomble et al., 2009; O'Toole et al., 2003; Trépout et al., 2018; Vaughan and Gull, 2016). The flagellum remains attached to the cell body *via* a junctional complex known as the flagellar attachment zone (FAZ) (Sunter and Gull, 2016). A set of four specialized microtubules (the microtubule quartet MtQ) nucleates between the mature (BB) and the pro-basal bodies (pBB), wraps around the FP, continues along the flagellar pocket collar (FPC) to extend up to the anterior end of the cell body (Gheiratmand et al., 2013; Robinson et al., 1995; Taylor and Godfrey, 1969).

PCF and BSF divide slightly differently but share the same cytokinesis stages characterized by the duplication of the single-copy organelles and their segregation leading to two daughter cells (schematized in Fig. S1a and 1b, respectively) (Vickerman, 1962; Sinclair and de Graffenried, 2019; Wheeler et al., 2013; Sherwin et al., 1989; Robinson et al., 1995; Farr and Gull, 2012). Those events are associated chronologically with pro-BB maturation, new flagellum growth, BBs segregation, and finally, cytokinesis combined with abscission (Fig. S1) (Wheeler et al., 2013; Wheeler et al., 2019). In *T. brucei*, the first noticeable events of the cell cycle are BB maturation, the nucleation of a new MtQ and the biogenesis of a new flagellum (Lacomble et al., 2009; Lacomble et al., 2010). Tight regulation of these events is critical for the parasite in

ensuring the correct position of the fold which determines the shape and form of the daughter cells and thereafter furrow ingression (Lacomble et al., 2010). The evolutionarily conserved protein kinases TbAUK1 (Aurora B kinase 1) and TbPLK (Polo-like kinase) may be involved in BB segregation (Ikeda and de Graffenried, 2012) while TbNRKC (NIMA related kinase C) is involved in replication and segregation and TbLRTP is involved in their replication (Morgan et al., 2005; Pradel et al., 2006). TbPLK has been shown to interact with numerous trypanosome-specific proteins including the cytokinesis regulator TOEFAZ1/CIF1 protein (McAllaster et al., 2015; Zhou et al., 2016a). TOEFAZ1/CIF accumulates at the new FAZ tip in a complex with the CIF2 and CIF3 proteins, all involved in cytokinesis furrow initiation (Zhou et al., 2016a; Kurasawa et al., 2018; Kurasawa et al., 2022). Contrary to most higher eukaryotes that rely on a contractile actomyosin ring, abscission in *T. brucei* requires flagellar movements (Broadhead et al., 2006; Ralston et al., 2006) or an undiscovered membrane fission mechanism (Farr and Gull, 2012).

In eukaryotic cells, centrioles are structures with a diameter of approximately 250 nm and with a length ranging between 150-500 nm (Winey and O'Toole, 2014). In a pair of centrioles, only the mother centriole (MC, *i.e* the mature centriole) bears distal appendages distal (DAs) and sub-distal appendages (SDAs) (Hatch and Stearns, 2010). The DAs are shaped as radial nine-fold twisted arrangement structures with fibrous located centrally and symmetrically at the distal end of the mother centriole. Each DA is associated with one of the centriole triplets with an angle of about 50 degrees (Uzbekov and Alieva, 2018). SDAs are conical-shaped structures linked to the centrosomal barrel by two axonemal microtubules triplets (Paintrand et al., 1992; Uzbekov and Alieva, 2018; Winey and O'Toole, 2014). These appendages (DA and SDA) are required for ciliogenesis and MC transformation into a basal body (BB) (Hall and Hehnly, 2021; Jana et al., 2014; Paintrand et al., 1992). MC and BB are similar in structure and function and the transition fibers that correspond to the DAs of the MC extend from the BB and connect to the plasma

membrane to initiate ciliogenesis (Hall and Hehnly, 2021; Kobayashi and Dynlacht, 2011; Kumar and Reiter, 2021; Paintrand et al., 1992; Pearson, 2014). The TF provide a physical demarcation of the flagellum/cilium compartment from the rest of the cell, allowing the recruitment and selective transport of proteins by the IFT machinery, essential for axoneme elongation and maintenance (Reiter et al., 2012; Wei et al., 2015). TF/DA components are well preserved among ciliated organisms such as CEP83, CEP89, CEP164 (centrosomal proteins), SCLT1 (sodium channel and clathrin linker 1), ANKRD26 (ankyrin repeat domain containing 26) that forms the backbone of blades, and FBF1 (Fas-Binding Factor 1) that localizes within the distal appendage matrix (DAM) between the appendage blades in proximity to the ciliary membrane (Bowler et al., 2019; Chong et al., 2020; Graser et al., 2007; Greenan et al., 2020; Hodges et al., 2010; Joo et al., 2013; Tanos et al., 2013; Tischer et al., 2021; Wei et al., 2013; Yang et al., 2018). Recently, a bioinformatics analysis identified orthologs of CEP164 and ANKRD26 in *T. brucei* (Tischer et al., 2021).

The trypanosome mature BB is composed of nine microtubule triplets followed by the transition fibres (TF) (Vaughan and Gull, 2016) and the transition zone (TZ) (Lacomble et al., 2009; Trépout et al., 2018; Vaughan and Gull, 2016). Together, the TF and TZ constitute the ciliary gate that serves as docking sites and regulators for intraflagellar transport and are involved in forming functional ciliary compartments in cilia and flagella (Reiter et al., 2012; Dean et al., 2016). To date, only two proteins have been identified as TF proteins in *T. brucei,* TbRP2 and CEP164C (Atkins et al., 2021; Stephan et al., 2007). In eukaryotes, RP2 and CEP164 proteins are conserved and embedded at the transitional fibres of the mature basal body where they provide an essential cilium/flagellum-specific function (Andre et al., 2014; Gonçalves and Pelletier, 2017; Graser et al., 2007; Reiter et al., 2012; Slaats et al., 2014; Stephan et al., 2007). In dividing trypanosome cells, TbRP2 is observed at the TF in both the old and the new flagella (Andre et al., 2014; Stephan et al., 2007) whilst CEP164C is present only on the TF of the old

flagellum (Atkins et al., 2021). RNA interference (RNAi) knockdown of TbRP2 leads to axonemal microtubule formation defect, disturbs the recruitment of TZ proteins and induces loss of tyrosinated α-tubulin on the mature BB without affecting the other microtubules (Stephan et al., 2007; Harmer et al., 2017; Atkins et al., 2021). The depletion of CEP164C induces dysregulation of the old flagellum growth due to a defect in the locking mechanism that regulates old and new flagella growth (Atkins et al., 2021).

Here, we have identified and characterized TFK1 (Transition Fibres Kinetoplastid-specific protein 1, Tb927.6.1180) as the first matrix transition fibre protein in *T. brucei* that is specific to kinetoplastids. Our high-resolution Ultrastructure Expansion Microscopy (U-ExM) data demonstrate new insight into the TF organization in *T. brucei* with distinct localization of TbRP2, CEP164C and TFK1. Our data reveal that TKF1 is composed of several predicted coiled-coil domains and an intrinsically disordered region (IDR). RNAi mediated knockdown of TFK1 in BSF induces previously undescribed cytokinesis defects that are ultimately lethal. Our results suggest an essential role for TFK1 in the coordination of certain cytoskeleton components during cell division of the bloodstream form *T. brucei*.

Results

TFK1 (Tb927.6.1180) is a kinetoplastid-specific coiled-coil protein

Tb927.6.1180 protein (ProteinID: XP_845240.1) was first identified as a potential BILBO1 binding partner, with a low interaction reliability predicted biological score, in *T. brucei* 927 genomic yeast two-hybrid screen (Hybrigenics), using BILBO1 as bait (Albisetti et al., 2017). Here, we identified Tb927.6.1180 as a novel basal body protein and designated it as TFK1 for Transition Fibres Kinetoplastid-specific protein 1. TFK1 is a 141.19 kDa protein consisting of 1271 amino acids with a calculated pI of 5.25 encoded by a single-copy gene located on

chromosome 6 (Fig.1A). TFK1 primary structure is composed of three distinct regions, (i) an N-terminal region (aa 1-74) with no predicted function, (ii) a large central region (aa 76-802) consisting of two coiled-coil regions CC1 (aa 76 to 536) and CC2 (aa 537-802), and (iii) a C-terminal region (aa 803-1271) predicted as an intrinsically disordered region (IDR) (Fig. 1A). Further, the presence of the coiled-coil and IDR domains suggests that TFK1 could form a homodimer and interact with other protein partners (Barbar and Nyarko, 2015; Kuhn et al., 2014; Uversky, 2013). Orthologs searches using BLAST-P, PSI-BLAST and HMMER (Altschul, 1997; Altschul et al., 2005; Finn et al., 2011) identified orthologs but only in the Kinetoplastea class with a conserved gene synteny. The TFK1 orthologs have an estimated molecular weight ranging from 118.41 to 160.11 kDa (for *Phytomonas* sp. and *T. vivax* respectively). A multiple sequence alignment using ClustalOmega identified the three conserved main regions (N-terminal domain, coiled-coil domain and IDR) among the TFK1 orthologs (Fig. S2) (Madeira et al., 2019).

TFK1 is located on the mature basal body

To localize TFK1, we generated a mouse monoclonal antibody (anti-TFK1) against the full-length purified TFK1 protein (Fig. S3A, B). Immunoblots of *T. brucei* cell lysates showed that anti-TFK1 recognized the wild-type TFK1 protein (141.19 KDa) in PCF and BSF forms (Fig. 1B) as well as an endogenously N-terminal TY1-tagged version of TFK1 (152.9 kDa) generated following the protocol described in (Dean et al., 2015) (Fig. S3C, D). The anti-TFK1 labelling revealed a major band at the expected size but also several other bands in both PCF and BSF (Fig. 1B). These bands diminished after TFK1 RNA interference (RNAi) knockdown experiments (described below) (Fig. S3C, D) and could reflect the phosphorylation status of the serines S898, S906, S1104 and S919 identified in phosphoproteomic analyses (Nett et al., 2009; Urbaniak et al., 2013), or due to proteolysis during cell lysis due to the presence of potential cleavage sites in the C-terminal domain of

TFK1. As previously observed on the TrypTag Genome-wide Protein Localization Resource that localized an endogenously N-terminal mNeonGreen-tagged form of TFK 1 in the BB area (Dean et al., 2016), our anti-TFK1 labelling was observed as two dots close to the kinetoplast in whole cells but also in detergent-extracted cytoskeletons of PCF and BSF cells (Fig. S3E and Fig. 1Ca respectively). This labelling co-localized with an anti-HA tag labelling of endogenously tagged TFK1$_{::HA}$ (Fig. S3E). The presence of a N-terminus or C-terminus tags did not affect the TFK1 localization (Fig. S3E). Importantly, this labelling was also maintained on detergent-extracted cytoskeletons of PCF and BSF cells indicating that the TFK1 protein is a cytoskeleton-associated protein localizing on or close to the basal bodies (Fig. 1Ca).

Further analysis of the immuno-labelling using the anti-TFK1 showed that TFK1 is present throughout the cell cycle at the base of both the old and the new flagellum in PCF and BSF (Fig. 1C). We thus wanted to co-label TFK1 with the BBs and flagellum-associated cytoskeleton protein markers BLD10, FTZC, CEP164C, TbRP2 and BILBO1. BLD10 is a conserved cartwheel protein (Carvalho-Santos et al., 2010) that stabilizes the 9-fold symmetry of the centriole in Chlamydomonas (Hiraki et al., 2007; Matsuura et al., 2004) and controls the formation of the flagellum central pair in Drosophila spermatozoid (Carvalho-Santos et al., 2012). BLD10 was also identified by bioinformatics and proximity-dependent biotin identification as a *T. brucei* basal body component (Dang et al., 2017). BLD10 localizes at both the mature and the immature BB throughout the cell cycle (Dang et al., 2017; Geimer and Melkonian, 2004). FTZC (for flagellar transition zone component) is a *T. brucei* specific protein localized at the perimeter of the transition zone (TZ) and thus can be used to localize the mature BB (Bringaud et al., 2000; Gorilak et al., 2021). CEP164C is a TFs protein that plays a role in the regulation of the *T. brucei* old flagellum length (Atkins et al., 2021) and TbRP2 is an alpha-tubulin binding and TFs protein involved in flagellum structure (Stephan et al., 2007) and in targeting of the ciliary gates TbMKS1 and TbMKS6 proteins (Andre et al.,

2014). TbBILBO1 is one of the components of the flagellar pocket collar (FPC), a cytoskeleton structure distal to the transition zone that maintains the flagellar pocket enclosed around the flagellum (Bonhivers et al., 2008). BILBO1 is also present at the BB and most probably along the MtQ between the BBs and the FPC (Broster Reix et al., 2021a; Perdomo et al., 2022). To carry out these co-labelling experiments we generated PCF cell lines expressing endogenous N-terminal 10xTY1 tagged TFK1 ($_{TY1::}$TFK1). To label the transition fibres, we generated a cell line expressing endogenous $_{TY1::}$TbRP2, and used a $_{mNeonGreen::}$CEP164C expressing PCF cell line (Atkins et al., 2021). Immunofluorescence assays in both PCF and BSF using anti-BLD10 (Dang et al., 2017) showed that despite close labelling, TFK1 does not co-localize with this BBs markers (Fig. 1Da and Fig. S4Aa) and is proximal to the FTZC labelling and to the FPC marker (BILBO1) (Fig. 1Db, c and Fig. S4Ab, c respectively). Interestingly, TFK1 co-localized, at least partially, with the two TF proteins TbRP2 and CEP164C (Fig. 1Dd and e, respectively).

TFK1 is a transition fibre protein

To analyze in more detail the basal bodies localization of TFK1 by increasing the spatial resolution, we used Ultrastructure Expansion Microscopy (U-ExM) (Amodeo et al., 2021; Gambarotto et al., 2021). TFK1$_{::HA}$ was co-labelled on detergent-extracted PCF cells with the cytoskeletal markers described above (Fig. 2). TFK1 appears as one set of nine individual dots organized in a circular fashion (Fig. 2Aa). This circular arrangement had average diameters of 1617 nm (inner) and 2533 nm (outer) which, after taking into account the expansion factor, indicates average diameters of 356 nm (inner) and 558 nm (outer) (n=10) (Fig. S4B). The BBs can be identified by BLD10 labelling which forms the cartwheel structure of the mature BB and the pro-BB (pBB) (Dang et al., 2017), while in G1 trypanosome cells CEP164C labels the mature BB only (Atkins et al., 2021). At the early SK1N (Early kinetoplast S phase) stage of the cell cycle, the BB and pro-BB or the maturing

pro-BB (pBBm) are identified by BLD10 labelling (Dang et al., 2017). In these cells, TFK1 is only present on the mature basal body (BB) (Fig. 2Aa, e), and at a slightly later stage is also on the maturing pro-BB (pBBm) as shown with the BLD10 co-labelling (Fig. 2Ba, b). To distinguish between the BB and the maturing pro-BB, we used the $_{mNG::}$CEP164C expressing cell line (Atkins et al., 2021). In Fig. 2Ab, we show the first high-resolution localization of CEP164C that adopts punctuated radial arrangement, in agreement with the arrangement on TFs shown for the human ortholog CEP164 (Yang et al., 2018). Also, CEP164C labelling appears unregular in intensity and positioning suggesting a localization on different planes (Fig. 2Ab) similarly to the organization described for human ortholog CEP164 forming the backbone of the nine DA blades (Yang et al., 2018). Interestingly, the co-labelling of TFK1 with CEP164C demonstrates that TFK1 is associated with the CEP164C-positive mature basal body labelling suggesting that TFK1 is a mature BB or maturing pro-BB protein (Fig. 2Ab). Interestingly, it is noticeable that the gaps present between the CEP164C dots are filled with the TFK1 dots as observed on the top and side views (Fig. 2Ab, f) suggesting that TFK1 and CEP164C belong to two different compartments of the TF. In addition, this is supported by the fact that in PCF, the knockdown CEP164C RNAi does not affect the localization of TFK1 at the TFs (Fig. S8b).

Remarkably, co-labelling with $_{TY1::}$TbRP2 revealed a continuous radial arrangement of TbRP2 somewhat smaller and distinct from the nine-dot arrangement of TFK1 (Fig. 2Ac). In addition, the side views (Fig. 2Ag and Fig. 2Bd) confirmed that TbRP2 and TFK1 are on separate structures with TFK1 distal to TbRP2 (relative to the kinetoplast oriented downwards in Fig. 2 in the U-ExM images). At the early SK1N (Early kinetoplast S phase) stage of the cell cycle, BB and the maturation of the pro-BB are identified by BLD10 labelling (Fig. 2Bb). The U-ExM showed that TFK1 labelling is observed once the pro-BB matures. Indeed, the BLD10 labelling in figure 2Bb shows a newly maturing BB that is also associated to TFK1 labelling (indicated with an asterisk, Fig. 2Bb). This is confirmed by the TbRP2 labelling that

shows a newly TbRP2-positive structure associated to TFK1 labelling (Fig. 2Bd, asterisk) and the TFK1 labelling (Fig. 2Bf, asterisk) close to the base of the presumed pro-BB MtQ labelled with BILBO1 (Broster Reix et al., 2021a), suggesting they could be markers for an event of maturation of the pro-BB.

Subsequent immuno-gold electron microscopy images of thin sections from detergent-extracted, pre-labelled, cytoskeletons using anti-TFK1 confirmed the precise location of TFK1 on the TF (Fig. 3). On longitudinal sections (micrographs A and B), the gold particles are observed at the tip of the TF region, at the base of the transition zone subtending the flagellum. This was clearly observed on transversal sections where the nine-bladed TF structures are radiating around the BB but the immuno-gold particles are distal to the blades (Fig. 3C and D). In order to determine the exact location, we measured the distance between the basal body's center and the immuno-gold labelling on transversal sections revealing a length of 172±26 nm (n=28, white arrow in Fig. 3C and Table S1). In addition, some immuno-gold labelling was observed close to a pro-BB suggesting that it has already entered maturation (Fig. 3D) in agreement with our previous observation by U-ExM (Fig. 2Bb, d, f, indicated by an asterisk).

Taken together, our data indicate that TFK1 is a cytoskeleton-associated protein expressed in PCF and BSF parasites throughout the cell cycle. TFK1 is a marker of BB maturation localizing at the tip of the TF, with a spatial organization that differs from those of the only other two *T. brucei* described TF proteins, CEP164C and TbRP2 and is schematized in Fig. 4.

The TFK1 CC1 coiled-coil domain is sufficient to target to the transition fibre zone

To further characterize the three main regions of the TFK1 protein, we generated PCF cell lines tetracycline-inducible (Wirtz et al., 1999) for the ectopic expression of C-terminus 3xmyc-tagged TFK1 ($TFK1_{::myc}$) and truncated forms of TFK1 (truncations T1 to T5

described in Fig. 5A) in the TFK1$_{::HA}$ background. The proteins were detected by immunofluorescence with anti-HA for the endogenous TFK1$_{::HA}$ and anti-myc for the ectopic copies (Fig. 5B and S5B), and with anti-myc by western blotting (Fig. S5A). The myc-tagged proteins were all expressed after tetracycline induction (Fig. S5A). The expression of the ectopic proteins was induced with tetracycline for 24 h and the cells were subjected to immunofluorescence and western blotting (24 h and 48 h induction) (Fig. 5B and S5A, B). TFK1$_{::myc}$ co-localized with endogenous TFK1$_{::HA}$ on detergent-extracted cytoskeletons (Fig. 5Bc) with no cytoplasmic pool as observed on whole cells labelling (Fig. S5Bb). The truncations T1$_{::myc}$ (N-terminal domain) and T3$_{::myc}$ (IDR) both lacking the CC region were observed as a cytoplasmic pool in whole cells (Fig. 5Bd, f) that was removed in detergent-extracted cytoskeleton (Fig. S5Bc, d) suggesting that they are not required or sufficient for TFs targeting. On the contrary, the large CC domain (composed of CC1 and CC2, T2$_{::myc}$) co-localized on the TF, together with the endogenous TFK1$_{::HA}$ on extracted cells (Fig. 5Be). To further uncover the exact region of the CC domain involved in the TFs targeting, the CC1 (T4$_{::myc}$) and CC2 (T5$_{::myc}$) domains were expressed. Interestingly, we observed that the CC1 domain localized to TF (Fig. 5Bg) whilst the CC2 domain was observed in the cytoplasm in whole cells (Fig. 5Bh) and was removed in detergent-extracted cytoskeleton (Fig. S5Be). These data show that the highly conserved coiled-coil domain CC1 (aa 76-536) is sufficient to address TFK1 to the TF.

The CC1 coiled-coil domain is involved in TFK1-TFK1 interaction

Because the CC and IDR domains can be involved in protein-protein interactions, we used the Yeast Two-Hybrid (Y2H) approach to determine if they could be involved in TFK1-TFK1 interaction (Fig. 5C). Y2H assays demonstrated that TFK1 can form homodimers as cell growth was obtained for full-length TFK1 x full-length TFK1 (FL x FL, Fig. 5C). To identify

which domain was involved in this interaction, the truncations T1 to T5 were tested against the full-length TFK1. Only the truncations T2 (CC1+CC2) and T4 (CC1) interacted with TFK1 demonstrating that the conserved coiled-coil domain CC1 (aa 75-536) is implicated in the formation of homodimers. This interaction between the full-length TFK1 and its CC1 domain should be considered into account in our immunolocalization of CC1 *in vivo* to the TFs (Fig. 5Bg) that could be a downstream result of its interaction with the endogenous full-length TFK1 protein. Interestingly, dimerization - oligomerization was conceptualized for the recruitment of the CC-rich domain of human CEP164 to the centriole (Mennella et al., 2012; Yang et al., 2018).

TFK1 Knockdown induces cell cycle arrest and cell death

To assess the function of TFK1, a tetracycline-inducible RNAi knockdown approach was used in the $_{TY1::}$TFK1 background PCF and BSF cells (Wirtz et al., 1999). No phenotypes were observed in PCF over the time of RNAi induction despite the decrease of protein level observed by western blot (Fig. S6A, B). However, absence of phenotypes might be due to incomplete depletion of TFK1 as the protein was still detected by western blotting after 96 h of induction (Fig. S6B). In contrast, in BSF cells, a growth arrest was observed 48 h post RNAi induction followed by cell death within 72 h (Fig. 6A). TFK1 protein level during RNAi induction was investigated by western blot and showed a strong decrease at 24 h post-induction and very low detection at 48 h post-induction using both anti-TY1 (left panel) and anti-TFK1 (right panel) (Fig. 6B). In addition, TFK1 protein depletion was also observed by immunofluorescence as the protein was not detected after 24 h of induction (Fig. 6C). Since TFK1 RNAi is lethal in BSF, we assessed cell cycle progression at different time-points of induction by using DAPI to stain the kinetoplast (K) and the nucleus (N) DNA and quantify their numbers (Fig. 6D). At 24 h post induction (+ Tet 24 h), the percentage of 1K1N cells

decreased from 76% to ~ 52%, together with an accumulation of 2K2N cells that increased from 8% to ~ 22% (Fig. 6D Table). There was also appearance of abnormal cells such as 1K2N (~ 3%), XKXN (X≥3) (~ 8%) and "round" dead/dying cells (~ 3.4%) (Fig. 6D Histogram). Interestingly, the percentage of 2K2N cells at 48 h post induction (~ 9%) was similar to the non-induced 2K2N population (~8%) whilst the abnormal population of XKXN increased to ~ 43% (Fig. 6D Histogram) suggesting a downstream effect of the increase of the 2K2N cell population at 24 h of induction (~22%).

Overall, these results indicate that TFK1 is essential in BSF *T. brucei* and its depletion induces cytokinesis defects without affecting mitosis leading to cells with an abnormal number of kinetoplasts and nuclei.

Knockdown of TFK1 affects cleavage fold completion leading to "locked posterior-posterior" and "tandem-cell" phenotypes in bloodstream forms

To study further the phenotypes induced by TFK1 RNAi in BSF and to preserve the morphology of the cells, including the cytoplasmic bridge, WT or TFK1 RNAi non-induced and induced cells were fixed in the culture medium, stained with DAPI and observed by phase contrast. The number of kinetoplasts (arrow heads) and nuclei (asterisk) were followed along the cell cycle stages for the non-induced cells (Fig. 7Aa). At the 2K2N stage (Fig. 7Aa 2K2N, cytokinesis and abscission) cytokinesis progresses with the formation of a division cleft (dashed line) leading to the abscission stage where the two daughter cells are connected with the cytoplasmic bridge (arrow) in a posterior end-to-posterior end manner. Finally, the bridge is broken by flagellum-driven motility of both daughter cells (Wheeler et al., 2013). To investigate this division process during TFK1 depletion by RNAi, 24h-induced cells were similarly prepared and observed, with a particular attention to the 2K2N cells (Fig. 7Ab and c). No phenotype was observed in the first cell cycle stages (1K1N, S1K1N and 2K1N).

However, in the BSF 2K2N stage two main cytokinesis defect phenotypes were observed, (1) an increase in the 2K2N cell population of cells that are connected by their posterior ends with a cytoplasmic bridge at the abscission stage that we named the "locked posterior-to-posterior" phenotype (from 17.6% in WT cells to 30.2% in induced cells) (Fig.7Ab, d) and (2) an unusual KNKN organization that we named the "tandem-cells" phenotype that was never observed in WT cells and reached 13.4% of the 2K2N induced cell population (Fig. 7Ac, d). Therefore, the normal population of 2K2N cells, with a KKNN organization, decreased significantly (from 82.4% in WT cells to 56.3% in induced cells) (Fig. 7Aa, d).

In the "locked posterior-to-posterior" phenotype, TFK1 RNAi induced BSF cells progressed normally through the cell cycle up to the abscission step. At the 2K2N stage an apparently proper fold and two nascent posterior ends were formed in the 2K2N cells (Fig. 7Ab, 2K2N cytokinesis), as well as the furrow ingression and pre-abscission by the presence of cytoplasmic bridge in a posterior-to-posterior organization (Fig. 7Ab, 2K2N no abscission). However, these cells were not able to complete abscission before asynchronous mitosis cycles occurs as shown by the number of DAPI-stained kinetoplasts and nuclei (Fig. 7Ab, XKXN no abscission). Both attached daughter cells were asynchronous with an unequal number of flagella visualized by PFR labelling (Fig. 7Ce and f). SEM analysis supported these observations, showing two daughter cells connected by their posterior ends (Fig. 7D arrows, locked posterior-to-posterior).

In the previously undescribed 2K2N "tandem-cells" phenotype, the organization of the kinetoplasts and nuclei resembles the one in PCF cells with a KNKN distribution instead of a KKNN distribution (Fig. 7Ac, 2K2N). This cell population was never observed in non-induced cells but represented 13.4% of the 2K2N population of 24h-induced TFK1 RNAi cells (Fig. 7Ad, "tandem-cells"). The observation of these cells after detergent-extraction showed in more detail that the sub-pellicular microtubule cytoskeleton of both WT and tandem-cells form a continuous corset for the two daughter cells (Fig. 7Bb). However, the

tandem-cells have clearly misplaced new kinetoplast and new flagella (Fig. 7Bb). This could lead to or is the result of abnormal fold positioning (Fig. 7Bb) compared to the non-induced condition (Fig. 7Ba) where the fold terminates closer to the posterior end in BSF and defines the two nascent posterior ends (Wheeler et al., 2013). In induced cells, the DNA content of the two cells continued to replicate indicating a restart in cell cycle and leading to XKXN and multi-flagellated cells, as shown with the flagella labelling with the anti-PFR antibody (Fig. 7Cb, c), without achieving cytokinesis (Fig. 7Ac XK2N, XKXN). Interestingly, whole cell and cytoskeleton preparations revealed the existence of a structure resembling a bridge that prevented daughter cell separation (Fig. 7Ac, arrows XNXN and Fig. 7Cc). Similar observations were made by scanning electron microscopy (SEM) showing this atypical organization of "tandem-cells" in BSF (Fig. 7D, arrows tandem-cells).

In TFK1 RNAi induced cells, defects neither in the basal bodies (as labelled with anti-BLD10) (Fig. S7Ab) nor in flagellum structure (as observed on thin section by electron microcopy) were observed (Fig. S7Ab). Likewise, the cytoskeleton-associated structures such as the flagellum (visualized by a PFR signal, Fig. 7C) and the flagellar attachment zone (FAZ, labelled with the anti-FAZ L3B2 monoclonal, Fig. 7C), and the flagellar pocket collar (labelled with anti-BILBO1, Fig. S7Ad, Ba and c) were unaffected by TFK1 knockdown. Comparison of electron microscopy images of thin sections from non-induced and 24 h induced TFK1 RNAi BSF cells showed no obvious difference in the overall ultrastructure of the cytoskeleton (Fig. S7B). PFR length was also measured in non-induced and induced TFK1 RNAi conditions and showed no change in the length of the flagella, suggesting a proper flagellum formation (Fig. S7C). We also compared the diameter of the TF area after TFK1 RNAi knockdown by measuring the distance between the two sides of the flagellar pocket at the base of the flagella (indicated by a white double-arrow on Fig. S7Bc), but this showed no significant differences between induced and non-induced cells (Fig. S7D).

Furthermore, on cells induced for the RNAi knockdown of the flagellar pocket collar protein BILBO1 that display a detached new flagellum and no FP biogenesis (Bonhivers et al., 2008), TFK1 labelling remains present at the BB (Fig. S8A). This suggests that absence of FP formation does not affect the localization and most probably the function of TFK1.

Taken together, our data demonstrated that TFK1 is a TF fiber protein. Co-localization of TFK1 with CEP164C and TbRP2 suggest that TFK1 is the first TF matrix protein identified in trypanosomes and is essential for the last stages of the cell cycle of the *T. brucei* BSF (localization schematised in Fig. 8). Depending on the stage of progression in the cell cycle, TFK1 knockdown leads (i) a misplacement of the new BB resulting in a KNKN phenotype that we named "tandem-cells" that has not been reported previously in BSF and, (ii) to a defect in the abscission that has previously been described in PCF described for other cell cycle proteins (Sinclair-Davis et al., 2017).

Discussion

Trypanosome basal bodies act as vital master organizers of the cytoskeleton, organelles and flagellum positioning (Lacomble et al., 2009; Lacomble et al., 2010). During maturation, the pro-BB acquires appendages, essential structures for docking to the plasma membrane and recruitment of the intraflagellar transport proteins (IFT) (Stephan et al., 2007; Morga and Bastin, 2013; Wei et al., 2015; Bertiaux et al., 2018). These radial structures are comprised of nine distal appendages (DA)/transition fibres (FT) and nine sub-distal appendages (SDA) (Tanos et al., 2013; Vaughan and Gull, 2016; Garcia-Gonzalo and Reiter, 2017; Trépout et al., 2018; Yang et al., 2018). In this study, we identified TFK1 (Transition Fibre protein Kinetoplastid specific-1) as a novel TF component and BB maturation marker which is unique to kinetoplastea class and present throughout the trypanosome cell cycle in PCF and BSF.

TFK1, a component of the distal appendage matrix in the transition fibres

Only two TF proteins have been described in *T. brucei*, TbRP2 and CEP164C (Andre et al., 2014; Atkins et al., 2021; Stephan et al., 2007). Using Ultrastructure Expansion Microscopy (U-ExM), we show for the first time in *T. brucei* the high resolution localization of CEP164C, that adopts a radial arrangement of several dense dots similar to the labelling observed for human CEP164 (Yang et al., 2018), and of TbRP2 that is proximal to CEP164C. We show here that TFK1 is localized at the BB, is distal to TbRP2 and is organized as nine equidistant dots around the BB that fill the circumferential gaps of CEP164C arrangement without co-localization. Together with CEP164C and TbRP2, TFK1 is the third *bona fide* protein component of the trypanosome TFs.

Recent ultrastructural studies of the human TFs/DAs described in great details a cone-shaped architecture composed of nine distal appendage blades (DABs) that are embedded in the distal appendage matrix (DAM), also known as periciliary diffusion barrier (PCB) (Nachury, 2018), where FBF1 (Fas-Binding Factor 1) and IFT molecules localize (Yang et al., 2018). Our measurements reveal that the nine TFK1 dots define with an inner and an outer diameter of 356±28 nm and 558±58 respectively, similar to the diameters found for the human orthologs CEP164 (568±18 nm to 219±14 nm) and FBF1 (269±33 nm to 496±26 nm) on the DAs (Yang et al., 2018; Bowler et al., 2019; Katoh et al., 2020). Taken together, our data suggest that TFK1 may be present in the DAM structure similar to the FBF1 protein between the nine DABs composed of, among others, CEP164 (Yang et al., 2018). In addition, we show that the TFK1 immuno-gold labelling is located at 172±26 nm away from the BB's center, in agreement with the same distance of ~ 177 nm measured for mammalian centrioles (Bowler et al., 2019). This distance (or radius) is equivalent to a diameter of 344±51 nm. The diameter of the dense TF structures (the blades) observed in *T. brucei* by EM is in the range of 338 nm to 388 nm (Trépout et al., 2018) suggesting that TFK1 localizes at the distal end of the blades structure in the DAM as described for FBF1 (Wei et al., 2013; Yang et al., 2018).

We show, in BSF, that depletion of TFK1 does not affect BB structures *per se*, flagella structure and length or the diameter of the TF area, indicating that TFK1 is not involved in the biogenesis of these cytoskeletal structures. In comparison, Atkins and colleagues have shown that RNAi of CEP164C, in PCF, induces abnormal elongation of the old flagella, without altering its structure (Atkins et al., 2021). Within the same RNAi strain, we show that when CEP164C is depleted TFK1 protein is still detected at the TF (Fig. S8B). These results indicate that while the two proteins CEP164C and TFK1 are close on the TF, TFK1 localization is independent of CEP164C. This is similar to the absence of the human CEP164 at the DAB tips that did not affect the recruitment of FBF1 to the DAM (Yang et al., 2018) indicating a distinct role from other central components of the DAB (Yang et al., 2018). FBF1 is a DAM protein required for ciliogenesis, ciliary gating, centriole duplication and separation (Inoko et al., 2018; Tanos et al., 2013; Wei et al., 2013; Yang et al., 2018). Using BLAST-P, we searched for the FBF1 (isoform 1) human protein sequence (Q8TES7-1) ortholog in kinetoplastids and identified Tb926.6.4100 (Protein ID: XM_840435.1) with 11.6% similarity and 7.2% identity. Interestingly, Tb926.6.4100 was localized at the basal bodies by the TrypTag resource (Dean et al., 2016; Dean et al., 2017). DAM area could be composed of different proteins that play different functions, specific to the organism.

TFK1 is involved in furrow function in the BSF cell cycle

In BSF, TFK1 depletion induced a misregulation of the cell division cycle characterized by an arrest of cytokinesis at 2K2N stage leading to either a previously uncharacterized “tandem-cells” phenotype, with a KNKN arrangement along the posterior to anterior of the cell axis, or a "locked posterior-to-posterior" phenotype (NKKN), which corresponded to an abscission arrest or delay leading to rapid cell death. Nevertheless, in both phenotypes, mitosis still occurred. However, no phenotype was observed in PCF RNAi cells. It is well documented that depletion of proteins involved in structural integrity and/or flagellum motility induces major defects in cytokinesis, which are frequently lethal in BSF (Broadhead et al., 2006;

Ralston et al., 2006; Dacheux et al., 2012; Wheeler et al., 2013; Dang et al., 2017; Zhang et al., 2019). In addition and confirming an important phenomenon observed by us, several studies show that RNAi knockdown of the same protein can produce different phenotypes in PCF and BSF life stages (Hammarton et al., 2003; Kumar and Wang, 2005; Broadhead et al., 2006; Benz et al., 2012; Zhang et al., 2019; Lai et al., 2021; Morriswood et al., 2009; Broster Reix et al., 2021b). Our data demonstrate once again that the essentiality of a protein such as TFK1 can vary from one life-cycle stage to another in *T. brucei*.

Interestingly, the TFK1 RNAi "tandem-cells" phenotype obtained in BSF show the same KNKN arrangement of WT, PCF cells suggesting a role of TFK1 in BB placement. During the elongation of the new flagellum in BSF, the distal tip is connected to the cell body plasma membrane in the groove structure, which is present until the new flagellum extends beyond the anterior end of the cell (Hughes et al., 2013). The initiation of the division fold and the cleavage furrow corresponds to the resolving of the groove and to a significant reduction of the distance between the two kinetoplasts (Hughes et al., 2017; Tyler, 2001). In the KNKN "tandem-cells" phenotype, the new and old FAZ and the flagella grew properly but a stopping point for the elongation of the sub-pellicular microtubule corset and the separation of the flagella seemed to be missing as well as a starting point for the initiation of the cleavage furrow (Absalon et al., 2007; Davidge et al., 2006; Farr and Gull, 2012; Hughes et al., 2017; Robinson et al., 1995).

The exact molecular role of TFK1 is yet to be discovered but, TFK1, together with TbRP2 were identified by proximity-dependent biotinylation identification (BioID) as an interactor protein of TOEFAZ1/CIF1 (a key regulator of the cytokinetic furrow) but not CEP164C (Hilton et al., 2018). However, our Y2H assays did not show a direct interaction between TFK1 and TOEFAZ1/CIF1 (Fig. S8C) suggesting that TOEFAZ1/CIF comes in close proximity to TFK1 during its journey along the flagellum (McAllaster et al., 2015; Sinclair-

Davis et al., 2017; Zhou et al., 2016a) but do not interact. Moreover, TFK1 has been identified in the proteomic analyses of the immuno-isolated bi-lobe complex (Gheiratmand et al., 2013). Gheiratmand and colleagues have identified many other proteins localized on single-copy organelles such as the flagellum, the MtQ, the FPC, the kinetoplast, and the bi-lobe but neither TbRP2 nor CEP164C were identified in their analysis. This suggests that TFK1 could be specialized in interacting with some proteins that transit along the MtQ towards the bi-lobe and beyond.

Our study also shows that TFK1 depletion induces the blockage or delay of abscission, leading to the "locked posterior-to-posterior" phenotype, while allowing further rounds of mitosis.

TFK1, a candidate regulator of cytokinesis in bloodstream form

The studies of the trypanosome-specific key regulators (TOEFAZ1/CIF1, CIF2, CIF3, KLIF, FRW1) in the initiation of cytokinesis in *T. brucei* have shown that they are regulated by different mechanisms at different stages of the life cycle (BSF and PCF) (Zhou et al., 2016a; Zhou et al., 2016b; Zhou and Li, 2016; Hilton et al., 2018; Zhou et al., 2018). The two trypanosome-specific proteins KLIF and FRW1 are remarkable examples. Both were identified at the cell division fold and cleavage furrow (Hilton et al., 2018; Zhou et al., 2018). Although these two proteins are expressed in both forms, KLIFF is essential in PCF and FRW1 is essential in BSF (Hilton et al., 2018; Zhang et al., 2019). FRW1 is localized at the BBs and at the furrow ingression during cytokinesis but its depletion was not essential for survival in PCF. In contrast, in BSF, FRW1 has been detected as multiple punctate dots in the middle portion of the cells and its depletion was leading to defects in cytokinesis initiation and lethal (Zhang et al., 2019). The common underlying mechanism between the phenotypes

induced during the RNAi of TFK1 and of FRW1 could be the modification of the corset at a specific time point. This would first allow the initiation of the groove ingression that could be affected in the "tandem-cell" phenotype and second, to cut the cytoplasmic bridge, a cut that no longer occurs or is delayed in the "locked posterior-to-posterior" phenotype. The essential role of the centriole in cytokinesis and especially in the regulation of abscission has been described in mammalian cell lines. Migration of the centriole to the intercellular bridge (midbody) controls the release of microtubules and the completion of cell division. The authors suggest that this centrosome-dependent pathway may have been conserved during evolution (Jonsdottir et al., 2010; Piel et al., 2001). The centriole and basal body clearly have other, cryptic functions that to date have not clearly been elucidated.

In summary, our results describe TFK1 as a kinetoplastid specific protein and as a mature and maturing BB marker, localized on the transitional fibres. TFK1 is the third component of the transition fibre region, with TbRP2 and CEP164C, in *T. brucei*. TFK1 is displayed in a typical radial arrangement in the distal appendage matrix, as nine dense points between the molecules of CEP164C. TFK1 is essential for BSF, unlike PCF. Its depletion induces, on one hand, the absence of furrow associated with segregation of BBs similar to that of PCFs (KNKN) and on the other hand, leads to the blockage of abscission during cytokinesis in BSFs. These two processes maybe interlinked or have some degree of interdependency. Our results suggest an essential role of TFK1 in the segregation and positioning of BBs to ensure the shape of subsequent daughter cells. The role of TFK1 could be extended to other forms of the trypanosome life cycle, which exhibit different morphologies (trypomastigote and epimastigote) as well as a different positioning of the nucleus and basal bodies along the axis of the cell (Langousis and Hill, 2014; Varga et al., 2017; Zhang et al., 2019; Lemos et al., 2020).

Materials and Methods

In silico analysis

The TrypTag resource (http://tryptag.org) (Dean et al., 2016) localized previously Tb927.6.1180 (ProteinID: XP_845240.1) as a basal body protein. TFK1 orthologs were identified by walking BLAST-P, PSI-BLAST and HMMER (Altschul, 1997; Altschul et al., 2005; Altschul et al., 2005; Finn et al., 2011) using default parameters (standard databases, non-redundant protein sequences database, maximum target sequences 100, with short queries, expect threshold E-value of 0.05 (and 0.01), no maximum matches in a query range). A multiple sequence alignments using ClustalOmega identified three main regions where residues are conserved among the TFK1 orthologs (Madeira et al., 2019). Accession numbers of protein sequences used are: *Trypanosoma brucei* (XP_845240.1, Tb927.6.1180), *Trypanosoma brucei gambience* (XP_011773895.1, Tbg972.6.880), *Trypanosoma congolense* (CCC90840.1, TcIL3000_6_680), *Trypanosoma cruzi* (PWV00945.1, TcCLB.507603.120), *Trypanosoma vivax* (CCC48277, TvY486_0600680), *Leishmania major* (Q4QGT1, LmjF.12.0120), *Phytomonas sp*. (CCW65273.1, GSEM1_T00005970001), *Crithidia fasciculate* (CFAC1_010006900, CFAC1_06_0150Z). InterPro provided functional analysis primary and secondary structures of proteins (https://www.ebi.ac.uk/interpro/) (Blum et al., 2021).

Trypanosome cell lines, culture and transfection

Procyclic (PCF) cell line SmOx P427 (Poon et al., 2012) was grown in SDM-79 medium (GE Healthcare, G3344-3005) pH7.4 supplemented with 2 mg/mL hemin (Sigma Aldrich, H-5533), 26 µM sodium bicarbonate, 10 mM D-glucose, 3.5 mM L-glutamine, 5.3 mM L-proline, 0.9 mM sodium pyruvate, 3.4 mM L-threonine, 150 mM glutamic acid, 120 µM sodium acetate, 230 µM D-glucosamine, 10% fetal calf serum complement-deactivated at 56°C for 30 minutes (FBS; Gibco, 11573397), 1 $\mu g.mL^{-1}$ puromycin and incubated at 27°C.

Bloodstream (BSF) cell line SmOx B427 (Poon et al., 2012) was cultured in IMDM medium containing 10% foetal calf serum complement-deactivated at 56°C for 30 minutes (FBS; Gibco, 11573397), 36 mM sodium bicarbonate, 136 µg.mL^{-1} hypoxanthine, 39 µg.mL^{-1} thymidine, 110 µg.mL^{-1} sodium pyruvate, 28 µg.mL^{-1} bathocuproine, 0.25 mM β-mercaptoethanol, 1.7 mM L-cysteine, 62.5 µg.mL^{-1} kanamycin, 0.1 µg.mL^{-1} puromycin and incubated at 37°C with 5% CO_2. For transfection, cell lines were grown at 5-10x10^6 cells/mL, then 3x10^7 cells were electro-transfected using transfection buffer as previously described (Wirtz et al., 1999; Schumann Burkard et al., 2011) with 10 µg of linearized plasmid using NotI or PCR product using the program X-001 of the Nucleofector®II, AMAXA apparatus (Biosystems).

After transfection, clones were obtained by serial dilution and maintained in logarithmic phase growth at 2x10^6 cells.mL^{-1} for PCF and at 1x10^5 cells.mL^{-1} for BSF. Selection antibiotics were added to the media according to the transfected product. Phleomycin (5 µg.mL^{-1} for PCF and 2.5 µg.mL^{-1} for BSF) was added to the media of transfected cells to select for those harboring the pLew100-3cMyc and p2T7tiB constructs, blasticidin (20 µg.mL^{-1} for PCF and 10 µg.mL^{-1} for BSF) and hygromycin (25 µg.mL^{-1} for PCF and 5 µg.mL^{-1} for BSF) were added to select the transfected cells harboring endogenous tags using pPOT vectors (Dean et al., 2015). Gene expressions and RNAi induction in the parasites were induced with tetracycline at 10 µg.mL^{-1}. Growth curves representing logarithmic number of cells were calculated by counting the number of cells every 24 h using Mallassez counting chamber slides.

Plasmid construction

***E. coli* BL21 (DE3) expression vectors.** To produce the anti-TFK1 mouse monoclonal antibody, the TFK1 open reading frame was amplified from *T. brucei* 927 genomic DNA (Melville et al., 2000) and cloned between HindIII and BamHI restriction sites into pET28a+ (Novagen) in frame with a C-terminus 6-histidine tag.

Trypanosome vectors. To express the full-length TFK1 (aa 1-1271) and its truncations (T1: aa 1-74; T2: aa 75-802; T3: aa 803- 1271; T4: aa 75-536; T5: aa 537-802) in PCF, the fragments were amplified by PCR and cloned into HindIII and NdeI restrictions sites of the pLEW100-X-3cMyc in frame with the C-terminus 3xMyc tag (home-modified from Wirtz et al., 1999). For the RNAi experiments in PCF and BSF, the TFK1 corresponding fragment (466 - 976 bp) was cloned between XbaI and XhoI restriction sites of the twin promoters plasmid p2T7tiB (LaCount et al., 2002). For endogenous gene tagging, primers were designed as described in (Dean et al., 2015) and PCR was performed using pPOTv4 (for N-terminus 10-TY1 tagging , Blasticidin resistance) or pPOTv7 vector (for C-terminus 3-HA tagging, Hygromycin resistance) as template. The PCR product was then used for trypanosome transfection as described in (Dean et al., 2015).

Yeast-two-hybrid vectors. To express the full-length TFK1 (aa 1-1271) and its truncations (T1: aa 1-74; T2: aa 75-802; T3: aa 803-1271; T4: aa 75-536; T5: aa 537-802) in yeast for interaction test, the fragments were amplified and cloned into SmaI and BamHI restriction sites of the pGAD-T7 (Activating domain, Clontech) and into BamHI and NcoI restriction sites of the pGBK-T7 (Binding domain, Clontech).

Western blot analysis

Trypanosomes were collected, centrifuged at 1000 x g (PCF) or 800 x g (BSF) for 10 minutes, and washed in PBS for PCF and vPBS (136.9 mM NaCl, 3 mM KCl, 16 mM Na2HPO4, 3 mM KH2PO4, 45.9 mM sucrose, 10 mM glucose) for BSF. For whole cells, the number of

cells to be loaded per well were calculated, then re-suspended in protein sample buffer 2x, plus nuclease 250 $IU.mL^{-1}$ (Sigma Aldrich, Ref. E1014). For detergent-extracted cells (cytoskeletons), cells were washed and re-suspended in 1% NP40, 100 mM PIPES pH6.9, 1 mM $MgCl_2$ for 7 minutes. Cytoskeletons were checked by microscopy, then centrifuged at room temperature for 10 minutes at 1000 x g, washed in 100 mM PIPES pH6.9, 1 mM $MgCl_2$ and resuspended in 2x sample buffer. The samples were boiled at 100◦C for 5 min then stored at -20◦C until required. Ten percent SDS-PAGE gels were prepared and samples loaded at $5x10^6$ PCF or BSF trypanosome cells per well according to the experiment. Samples were separated according to manufacturer's recommendations then transferred in a semi-dry system (BIORAD Trans-Blot Semi-dry transfer cell 221BR54560) onto PVDF membrane and incubated with blocking solution (BS: 5% skimmed milk powder, 0.2% Tween-20 in TBS) for 1 hour. For detection of tagged/non-tagged protein expression in trypanosomes, an anti-tag antibody or an antibody against the native protein was diluted in blocking solution according to the recommendation and incubated with the membranes overnight at 4°C. Membranes were washed in TBS and then in BS before probing with a specific secondary antibody conjugated to Horse Radish Peroxidase (HRP) for 60 minutes at RT. The following antibodies were used as primaries: anti-TFK1 (mouse monoclonal IgG1 purified, 1:500), anti-HA (mouse monoclonal IgG1, Biolegend, 901513, 1:1,000), anti-TY1 (BB2 mouse monoclonal antibody IgG1, 1:100) (Bastin et al., 1996) and anti-cMyc (rabbit polyclonal, Sigma, C-3956, 1 : 1,000). Anti-Enolase (rabbit polyclonal, 1:70,000) (Hannaert et al., 2003) and anti-tubulin (TAT1 mouse monoclonal, 1:1,000) (Woods et al., 1989) were used as loading controls. The secondaries used were anti-mouse HRP, diluted 1:10,000 in BS (Jackson, sheep, 515-035-062) and anti-rabbit HRP, diluted 1:10,000 in BS (Sigma, goat, A9169). Revelation was carried out using Image Quant LAS 4000 (GE) or Chemidoc (Biorad).

Immunofluorescence assays

1mL of log-phase PCF cells were centrifuged for 10 minutes at 1000xg, washed in 1x PBS, then 30 µL was loaded onto poly-L-lysine 0.1% solution (Sigma-Aldrich, P8920) coated slides for 5 minutes to adhere. Whole cells were fixed in methanol at -20°C for at least 30 minutes. Cytoskeleton extraction was carried out with 0.25% NP40 (Igepal) in PIPES buffer (100 mM PIPES pH 6.8, 1 mM $MgCl_2$) for 5 minutes, washed twice in PIPES buffer and cytoskeletons were fixed with methanol as described in (Florimond et al., 2015). For BSF, 10 mL of log-phase cells were collected, centrifuged at 800 x g for 10 minutes, then washed in vPBS; whole cells were fixed in 2% formaldehyde directly in the medium for 10 minutes and then loaded onto poly-L-lysine 0.1% solution (P8920 Sigma-Aldrich) coated slides for 5 minutes to adhere and permeabilized by methanol immersion for 5 minutes (Wheeler et al., 2013). Cytoskeleton extraction was carried out with 0.25% NP40 (as described above). Fixed cells were then incubated for 1 hour with single or combination of antibodies diluted in PBS + 2% BSA: anti-HA mouse monoclonal antibody IgG1 (Biolegend, 901513, 1 : 1,000), anti-HA mouse monoclonal antibody IgG2a, (Genetex, GTX628902, 1 : 1,000) and anti-TY1 BB2 mouse purified monoclonal antibody IgG1 (1:1,000) (Bastin et al., 1996) were used as antibodies against tagged proteins, anti-cMyc (rabbit polyclonal, Sigma, C-3956, 1 : 1,000) to detect overexpressed proteins, anti-TFK1 mouse monoclonal purified antibody IgG1 was used to detect the native TFK1 protein (1:500), anti-BLD10 (1:1,000) (Dang et al., 2017) were used as pro- and mature basal bodies marker, anti-FTZC rabbit polyclonal antibody (1:10,000) (Bringaud et al., 2000) was used as a transition zone marker, anti-*Tb*BILBO1 rabbit polyclonal (amino-acids 1-110, 1:4,000) (Florimond et al., 2015), anti-PFR2 rabbit polyclonal antibody (1:200) (Kohl et al., 1999), anti-FAZ mouse monoclonal antibody L3B2 (1:1,000) a kind gift from K. Gull (Kohl et al., 1999), anti-mNeonGreen (rabbit polyclonal, Ximbio, 155278, 1 : 10,000), washed twice in PBS + 0.1% Tween20, then incubated 1 hour with the appropriate secondary antibodies diluted 1:100 in PBS + 2% BSA: anti-mouse IgG FITC-

conjugated (Jackson, 115-095-164), anti-rabbit Alexa fluor 594-conjugated (Molecular probes, A-11012), anti-mouse IgG1 Alexa fluor 594-conjugated (Molecular probes, A-21125), anti-mouse IgG2a Alexa fluor 488-conjugated (Molecular probes, A21131). Kinetoplasts and nuclei were stained with 10 μL DAPI (10μg/ml) in 1xPBS for 5 minutes and slides were mounted with Slowfade® Gold antifade reagent (Molecular Probes). Images were acquired on a Zeiss Imager Z1 microscope with Zeiss 100x oil objective (NA 1.4), using a Photometrics Coolsnap HQ2 camera and Metamorph software (Molecular Devices) and processed with ImageJ (Schneider et al., 2012).

Electron microscopy thin section

The non-induced and induced TFK1 RNAi knockdown BSF cell pellets were placed on the surface of a copper EM grid (400 mesh) that had been coated with formvar. Each grid was very quickly submersed in liquid propane precooled and held at -180°C by liquid nitrogen as described in (Blancard and Salin, 2017). Briefly, the loops were then transferred in a pre-cooled solution of 4% osmium tetroxide in dry acetone in a 1.8 ml polypropylene vial at -84°C for 72h (substitution), warmed gradually to room temperature (1h -30°C, 2h -15°C, 2h 4°C and 30 min room temperature) followed by three washes in dry acetone. The samples were infiltrated progressively with araldite (epoxy resin Fluka). Ultrathin sections were contrasted with lead citrate and observed at 80kV on a Hitachi 7650 transmission electron microscope.

Immuno-electron microscopy

500 mL of mid log phase procyclic SmOxP427 cell line endogenously + TFK1$_{::3HA}$ were harvested at 1,000 x g, for 5 minutes, washed twice with PBS by centrifugation and resuspended in PBS. Freshly glow-discharged, formvar and carbon-coated G2000-ni nickel grids (EMS) were floated on a droplet of cells for 15 minutes. Grids were then moved onto a

drop of 1% NP-40 in PEME buffer (100 mM PIPES pH 6.8, 1 mM $MgCl_2$, 0.1 mM EGTA) 5 minutes at RT to extract the cells. Cytoskeletons were washed twice (2 x 5 minutes) in PEME buffer at RT, equilibrated and blocked on 50 µL drops of 2% fish skin gelatin (Sigma-Aldrich G7041) or blocking buffer (0.5% BSA, 0.1% Tween20 in PBS), then incubated on 25 µL of primary antibody diluted in blocking buffer (primary antibody was used either alone, or mixed with a second primary antibody), 1 hour at room temperature (RT). Mouse IgG1 anti-TFK1 purified monoclonal antibody was diluted 1:500. Grids were blocked and incubated in secondary antibody for 1h at RT (goat anti-mouse GMTA 5 nm gold, BBInternational) 1:10 in 0.2% fish skin gelatin in PBS. Grids were blocked and fixed in 2.5% glutaraldehyde in 0.2% fish skin gelatin in PBS. Samples were negatively stained with 1% aurothioglucose (Sigma-Aldrich) (10 µl for 30 sec), Micrographs were taken on a Philips Tecnai 12 transmission electron microscope at 100 kV.

Ultrastructure Expansion Microscopy (U-ExM)

The protocol used to assay Ultrastructure Expansion Microscopy on trypanosome has been described, adapted and optimized from (Gambarotto et al., 2021) and described in the online protocol https://dx.doi.org/10.17504/protocols.io.bvwqn7dw. Briefly, $4x10^6$ cells of mid log phase procyclic SmOx cell line endogenously single tagged $TFK1_{::3HA,\ mNeonGreen::}CEP164C$ and double tagged $_{10TY1::}TbRP2$ + $TFK1_{::3HA\ and}$ loaded onto poly-L-lysine 0.1% solution (Sigma-Aldrich, P8920) coated 12mm coverslips in 24-well plate and cells left to adhere between 5 to 10 minutes. Cells were covered with 1 mL of activation solution (0.7% formaldehyde, 1% Acrylamide in PBS) for 4 h at 37°C with slow agitation. For the gelation step, coverslips were gently deposited on top of a 35 µl drop of MS solution (23% Sodium acrylate (AK scientific R624), 10% Acrylamide (Euromedex EU0060-A), 0.1% Bis-acrylamide (Euromedex EU0560-A) in PBS) for 2 minutes then transferred to a 35 µl drop of MS, 0.5% TEMED (Euromedex 50406-A), 0.5% Ammonium persulfate (Euromedex EU0009-A) for 5 minutes

on ice then transferred at 37°C and incubated for 1 h in a moist chamber without agitation. The coverslips were then transferred in 6-well plate in 1 mL of denaturation solution (200 mM Sodium Dodecyl Sulfate, 200 mM Sodium chloride, 50 mM Tris pH 9.0) with agitation at RT for 15 minutes to detach the gel from the coverslip, that was then moved into a 1.5 mL Eppendorf centrifuge tube filled with denaturation solution and incubated at 95°C for one 90 minutes. Gels were expanded in large volumes of deionized water (twice 30 minutes then overnight) then incubated in a large volume of PBS for 10 minutes (three times). Small pieces of the gels were processed for immuno-labelling as follows. The gels were preincubated in blocking solution (PBS, 2% BSA, 0.2% Tween20) for 30 minutes at 37°C. The primary antibodies (rabbit polyclonal anti-BLD10 (Dang et al., 2017), 1:500 dilution; rabbit polyclonal anti-BILBO1, dilution 1:1,000 (Florimond et al., 2015); monoclonal mouse IgG1 anti-HA, 1:500 dilution (Biolegend, 901513); anti-HA (mouse monoclonal IgG2a, Genetex, GTX628902, 1 : 200); rabbit polyclonal anti- mNeonGreen (Ximbio, 155278), 1:1000 dilution, diluted in blocking solution were incubated for 3 h in the dark at 37°C with slow agitation. After three washes in blocking solution, gels were incubated with the secondary antibodies (anti-rabbit Alexa fluor 594-conjugated 1:500 dilution (Molecular probes, goat, A11012); anti-mouse Alexa fluor 488-conjugated dilution 1:500 (Molecular Probes, O-6380); anti-Mouse IgG1 specific Alexa fluor-594 conjugated 1:500 dilution (Molecular Probes, A21125); anti-Mouse IgG2a specific Alexa fluor 488-conjugated 1:500 (Molecular Probes, A21131) diluted in blocking solution for 3 h in the dark at 37°C with slow agitation. After three washes in blocking solution, gels were expanded in a large volume of deionized water (twice 30 minutes then overnight). An expansion factor was determined using the ratio between the size of the coverslip (12 mm) and the size of the gels after the first expansion. U-ExM images were acquired on a Zeiss Imager Z1 microscope with Zeiss 63x oil objectives (NA 1.4), using a Photometrics Coolsnap HQ2 camera and Metamorph software (Molecular Devices) and processed with ImageJ (Schneider et al., 2012).

Scanning Electron microscopy

BSF wild-type and BSF TFK1 24 h RNAi knockdown in endogenously tagged $_{10TY1::}$TFK1 were washed in vPBS and loaded onto poly-L-lysine 0.1% solution (Sigma-Aldrich, P8920) coated 12mm coverslips for 30 minutes. Samples were then fixed with glutaraldehyde (2.5%) in 0.1 M cacodylate buffer (pH 7.2) for 30 minutes at RT then overnight at 4°C. They were further washed twice in 0.1M cacodylate buffer and dehydrated in series of increasing ethanol concentrations (30 – 100%). Samples were dried via critical point drying (Leica EM CPD300, Austria). Afterwards, the coverslips were mounted onto stubs and coated with platinum, using a sputter coater (Q150T, Quorum Technologies, Kent, UK). Observations and images acquisitions were done at 3.5 kV, in "high vacuum" mode, using a GeminiSEM 300 FESEM (ZEISS Germany) and processed with ImageJ software.

Yeast-two-hybrid assay

The pGAD-T7 vectors were transformed in the appropriate yeast haploid cell line Y187 and the pGBK-T7 were transformed in the Y2HGold yeast haploid cell line. After production of diploid cells by yeast mating, interaction tests were carried out on SC- L – W – Histidine (His) media using drop test assay as described in the online protocol https://dx.doi.org/10.17504/protocols.io.btzenp3e (Isch et al., 2021).

Protein purification

E. coli BL21 (DE3) (Novagen) bacterial strain was transformed by heat shock method with pET28a+-TFK1-6His and grown in 200 mL of LB + kanamycin 50 mg/mL at 37°C and 250 rpm. When $OD_{600\ nm}$ ~0.6 was reached, cells were then subjected to cold shock on ice for 30 min. Protein expression of recombinant TFK1$_{::6His}$ was induced by adding 1 mM of isopropyl-β-D-thiogalactopyranoside for 3 h at 37°C overnight and 250 rpm. Cells were harvested by centrifugation and then resuspended in the lysis buffer containing 20 mM Tris-HCl, pH 7.4,

0.5 M NaCl, 20 mM imidazole and 10% (v/v) glycerol, protease Inhibitor Cocktail Set III Calbiochem (Ref. 539134-1 at 1:10,000 dilution). Cells were lysed by sonication and cell debris were pelleted by centrifugation (40,000 × g, 30 min, 4˚C). The supernatant was filtered (0.45-µm pore size, Amicon) and loaded onto a 1 ml HisTrapTMFF column (GE Healthcare) which was pre-equilibrated with the same lysis buffer. The column was washed with five column volumes (CV) of lysis running buffer and bound protein was eluted with 500 mM imidazole/running buffer with 10 CV. Elutions containing the highest concentration of purified recombinant TFK1$_{::6His}$ was run on 10% SDS-PAGE gel then stained with Coomassie Brilliant Blue (Instant BlueTM Expedeon Ltd). Purified recombinant TFK1$_{::6His}$ from a second identically loaded gel was transferred to PVDF membrane using a semi-dry transfer method (BIORAD) and a western blot was performed using anti-HIS (Sigma H-1029, mouse, 1:3,000) antibody to detect the His tag, followed by anti-mouse HRP conjugated (Jackson, 115-035-044, 1:10,000).

Monoclonal antibody production

Monoclonal antibodies were raised against purified TFK1$_{::6His}$ in 3 BALB/c mice using the protocol previously described by (Willcox et al., 2012). For immunization, 20 µg of recombinant TFK1$_{::6His}$ protein was emulsified with complete Freund's adjuvant and injected into each footpad of the back legs of each mouse. Twelve days later, the mice were boosted with 20 µg of recombinant TFK1::6His protein emulsified with incomplete Freund's adjuvant in the same conditions as the first injection. At day 15, after euthanasia of mice, popliteal lymph nodes were collected and B cells were extracted and fused with the myeloma partner P3U1 in PEG 1500 (Roche Diagnostic). Hybridomas were grown up to confluency and screened by indirect ELISA. Nunc Maxisorp flat 96-well plates were coated with 0.5 µg of TFK1 protein in carbonate buffer and saturated with 0.2% gelatin. After PBS (phosphate buffer saline) washes, 50 µl of hybridoma supernatants were added and incubated 1 hour at

37°C. After PBS washes, a secondary antibody HRP-conjugated anti-mouse IgG + IgM diluted 1:5000 (Jackson ImmunoResearch, 115-035-044) was incubated 1 hour at 37°C. Revelation was done by ABTS-H_2O_2 0.015% and the absorbance was measured at 405 nm, after PBS washes. Hybridomas, which secreted high levels of specific antibody against recombinant TFK1 protein were cloned by limiting dilutions and screened by immunofluorescence assay on endogenously tagged $TFK1_{::3HA}$ procyclic cells. The monoclonal IgG1 mouse antibody named anti-TFK1 was selected for its highly specific signal on immunofluorescence and western blot assays and used as described in this manuscript.

Ethics statement

Animal experiments have been performed in the conventional animal facilities of the University of Bordeaux (France) (approval number of B-33-036-917), with the approval of institutional guidelines determined by the local Ethical Committee of the University of Bordeaux and in conformity with the Ministry for Higher Education and Research and the French Committee of Genetic Engineering (approval number n °17621 -V5-2018112201234223).

Statistics

Experimental data for growth curves and cell count graphs is representative of n=3 independent experiments with values represented as Standard error of the Mean (SEM). Student t-test was used to determine the statistical significance between values given as $p < 0.005$.

Acknowledgments

We thank Pr. S. Dean (University of Warwick) for the pPOT vectors and trypanosome transfection protocol and Pr. K. Gull (University of Oxford) and Dr. P. Bastin (Institut Pasteur) for the BB2 antibody and the hybridoma. Dr M. Rojo., Dr J. Dompierre (IBGC) and Dr E. Bertiaux (University of Geneva) for expansion microscopy protocols. Dr. L. Zyin (University of Texas) for the anti-*Tb*BLD10 antibodie, Dr. J. Sunter (Oxford Brookes University) for the L3B2 antibody, Pr. K. Ersfeld (University of Bayreuth) for the 9E10 antibody, Dr. F. Bringaud (Université de Bordeaux) for the anti-Enolase and anti-FTZC antibodies, Dr. N. Biteau (Université de Bordeaux) for the anti-*Tb*PFR2 antibody, Pr. S. Vaughan (Oxford Brookes University) and Dr. P. Bastin (Institut Pasteur) for generous donation of $_{mNeonGreen::}$CEP164C endotagged and RNAi cell lines. This work was funded by the Centre National de la Recherche Scientifique, the Université de Bordeaux, the ANR-FWF PRCI [ANR-20-CE91-0003] to MB, the LabEx ParaFrap [ANR-11-LABX-0024] to DRR and the Fondation pour la Recherche Médicale to MMR and the Ministry of Higher Education, Research and Innovation

Competing interests

The authors declare no competing or financial interests.

Author contributions

Conceptualization: M.B., D.R.R., D.D.; Methodology: M.R.R., N.L., E.C., B.S., C.B., M.B., D.R.R., D.D.; Validation: M.B., D.R.R., D.D.; Formal Analysis: M.R.R., M.B., D.R.R., D.D; Investigation: M.B., D.R.R., D.D.; Resources: M.B., D.R.R., D.D.; Writing – original draft: M.R.R., D.D.; Writing - review and editing: M.R.R., M.B., D.R.R., D.D.; Supervision: D.D.; Project administration: M.B., D.R.R, D.D.; Funding acquisition: M.B., D.R.R.

Funding

This study was supported by the Centre National de la Recherche Scientifique, the Université de Bordeaux, Bordeaux-INP, the ANR-FWF PRCI [ANR-20-CE91-0003] to MB, the LabEx ParaFrap [ANR-11-LABX-0024] to DRR, the Fondation pour la Recherche Médicale (FDT202001010783) to MRR and the Ministry of Higher Education, Research and Innovation.

References

Absalon, S., Kohl, L., Branche, C., Blisnick, T., Toutirais, G., Rusconi, F., Cosson, J., Bonhivers, M., Robinson, D. and Bastin, P. (2007). Basal body positioning is controlled by flagellum formation in Trypanosoma brucei. *PloS One* 2, e437.

Albisetti, A., Florimond, C., Landrein, N., Vidilaseris, K., Eggenspieler, M., Lesigang, J., Dong, G., Robinson, D. R. and Bonhivers, M. (2017). Interaction between the flagellar pocket collar and the hook complex via a novel microtubule-binding protein in Trypanosoma brucei. *PLoS Pathog.* 13, e1006710.

Altschul, S. (1997). Gapped BLAST and PSI-BLAST: a new generation of protein database search programs. *Nucleic Acids Res.* 25, 3389–3402.

Altschul, S. F., Wootton, J. C., Gertz, E. M., Agarwala, R., Morgulis, A., Schaffer, A. A. and Yu, Y.-K. (2005). Protein database searches using compositionally adjusted substitution matrices. *FEBS J.* 272, 5101–5109.

Amodeo, S., Kalichava, A., Fradera-Sola, A., Bertiaux-Lequoy, E., Guichard, P., Butter, F. and Ochsenreiter, T. (2021). Characterization of the novel mitochondrial genome segregation factor TAP110 in Trypanosoma brucei. *J. Cell Sci.* 134, jcs254300.

Andre, J., Kerry, L., Qi, X., Hawkins, E., Drižytė, K., Ginger, M. L. and McKean, P. G. (2014). An Alternative Model for the Role of RP2 Protein in Flagellum Assembly in the African Trypanosome. *J. Biol. Chem.* 289, 464–475.

Atkins, M., Týč, J., Shafiq, S., Ahmed, M., Bertiaux, E., De Castro Neto, A. L., Sunter, J., Bastin, P., Dean, S. D. and Vaughan, S. (2021). CEP164C regulates flagellum length in stable flagella. *J. Cell Biol.* 220, e202001160.

Auty, H., Torr, S. J., Michoel, T., Jayaraman, S. and Morrison, L. J. (2015). Cattle trypanosomosis: the diversity of trypanosomes and implications for disease epidemiology and control: -EN- -FR- Trypanosomose bovine: la diversité des trypanosomes et ses conséquences sur l'épidémiologie de la maladie et sur son contrôle -ES- Tripanosomosis bovina: diversidad de tripanosomas y su influencia en la epidemiología y el control de la enfermedad. *Rev. Sci. Tech. OIE* 34, 587–598.

Barbar, E. and Nyarko, A. (2015). Polybivalency and disordered proteins in ordering macromolecular assemblies. *Semin. Cell Dev. Biol.* 37, 20–25.

Bastin, P., Bagherzadeh, Z., Matthews, K. R. and Gull, K. (1996). A novel epitope tag system to study protein targeting and organelle biogenesis in Trypanosoma brucei. *Mol. Biochem. Parasitol.* 77, 235–239.

Benz, C., Clucas, C., Mottram, J. C. and Hammarton, T. C. (2012). Cytokinesis in Bloodstream Stage Trypanosoma brucei Requires a Family of Katanins and Spastin. *PLoS ONE* 7, e30367.

Bertiaux, E., Mallet, A., Fort, C., Blisnick, T., Bonnefoy, S., Jung, J., Lemos, M., Marco, S., Vaughan, S., Trépout, S., et al. (2018). Bidirectional intraflagellar transport is restricted to two sets of microtubule doublets in the trypanosome flagellum. *J. Cell Biol.* 217, 4284–4297.

Blancard, C. and Salin, B. (2017). Plunge Freezing: A Tool for the Ultrastructural and Immunolocalization Studies of Suspension Cells in Transmission Electron Microscopy. *J. Vis. Exp.* 54874.

Blum, M., Chang, H.-Y., Chuguransky, S., Grego, T., Kandasaamy, S., Mitchell, A., Nuka, G., Paysan-Lafosse, T., Qureshi, M., Raj, S., et al. (2021). The InterPro protein families and domains database: 20 years on. *Nucleic Acids Res.* 49, D344–D354.

Bonhivers, M., Nowacki, S., Landrein, N. and Robinson, D. R. (2008). Biogenesis of the Trypanosome Endo-Exocytotic Organelle Is Cytoskeleton Mediated. *PLoS Biol.* 6, e105.

Bowler, M., Kong, D., Sun, S., Nanjundappa, R., Evans, L., Farmer, V., Holland, A., Mahjoub, M. R., Sui, H. and Loncarek, J. (2019). High-resolution characterization of centriole distal appendage morphology and dynamics by correlative STORM and electron microscopy. *Nat. Commun.* 10, 993.

Bringaud, F., Robinson, D. R., Barradeau, S., Biteau, N., Baltz, D. and Baltz, T. (2000). Characterization and disruption of a new Trypanosoma brucei repetitive flagellum protein, using double-stranded RNA inhibition. *Mol. Biochem. Parasitol.* 111, 283–297.

Broadhead, R., Dawe, H. R., Farr, H., Griffiths, S., Hart, S. R., Portman, N., Shaw, M. K., Ginger, M. L., Gaskell, S. J., McKean, P. G., et al. (2006). Flagellar motility is required for the viability of the bloodstream trypanosome. *Nature* 440, 224–227.

Broster Reix, C. E., Ramanantsalama, M. R., Di Primo, C., Minder, L., Bonhivers, M., Dacheux, D. and Robinson, D. R. (2021a). Intrabody-Induced Cell Death by Targeting the T. brucei Cytoskeletal Protein *Tb* BILBO1. *Microbiol. Spectr.* 9, e00915-21.

Broster Reix, C. E., Florimond, C., Cayrel, A., Mailhé, A., Agnero-Rigot, C., Landrein, N., Dacheux, D., Havlicek, K., Bonhivers, M., Morriswood, B., et al. (2021b). Bhalin, an Essential Cytoskeleton-Associated Protein of Trypanosoma brucei Linking TbBILBO1 of the Flagellar Pocket Collar with the Hook Complex. *Microorganisms* 9, 2334.

Büscher, P., Cecchi, G., Jamonneau, V. and Priotto, G. (2017). Human African trypanosomiasis. *The Lancet* 390, 2397–2409.

Carvalho-Santos, Z., Machado, P., Branco, P., Tavares-Cadete, F., Rodrigues-Martins, A., Pereira-Leal, J. B. and Bettencourt-Dias, M. (2010). Stepwise evolution of the centriole-assembly pathway. *J. Cell Sci.* 123, 1414–1426.

Carvalho-Santos, Z., Machado, P., Alvarez-Martins, I., Gouveia, S. M., Jana, S. C., Duarte, P., Amado, T., Branco, P., Freitas, M. C., Silva, S. T. N., et al. (2012). BLD10/CEP135 Is a Microtubule-Associated Protein that Controls the Formation of the Flagellum Central Microtubule Pair. *Dev. Cell* 23, 412–424.

Chong, W. M., Wang, W.-J., Lo, C.-H., Chiu, T.-Y., Chang, T.-J., Liu, Y.-P., Tanos, B., Mazo, G., Tsou, M.-F. B., Jane, W.-N., et al. (2020). Super-resolution microscopy reveals coupling between mammalian centriole subdistal appendages and distal appendages. *eLife* 9, e53580.

Dacheux, D., Landrein, N., Thonnus, M., Gilbert, G., Sahin, A., Wodrich, H., Robinson, D. R. and Bonhivers, M. (2012). A MAP6-related protein is present in protozoa and is involved in flagellum motility. *PloS One* 7, e31344.

Dang, H. Q., Zhou, Q., Rowlett, V. W., Hu, H., Lee, K. J., Margolin, W. and Li, Z. (2017). Proximity Interactions among Basal Body Components in Trypanosoma brucei Identify Novel Regulators of Basal Body Biogenesis and Inheritance. *mBio* 8,.

Davidge, J. A., Chambers, E., Dickinson, H. A., Towers, K., Ginger, M. L., McKean, P. G. and Gull, K. (2006). Trypanosome IFT mutants provide insight into the motor location for mobility of the flagella connector and flagellar membrane formation. *J. Cell Sci.* 119, 3935–3943.

Dean, S., Sunter, J., Wheeler, R. J., Hodkinson, I., Gluenz, E. and Gull, K. (2015). A toolkit enabling efficient, scalable and reproducible gene tagging in trypanosomatids. *Open Biol.* 5, 140197.

Dean, S., Moreira-Leite, F., Varga, V. and Gull, K. (2016). Cilium transition zone proteome reveals compartmentalization and differential dynamics of ciliopathy complexes. *Proc. Natl. Acad. Sci.* 113, E5135–E5143.

Dean, S., Sunter, J. D. and Wheeler, R. J. (2017). TrypTag.org: A Trypanosome Genome-wide Protein Localisation Resource. *Trends Parasitol.* 33, 80–82.

Farr, H. and Gull, K. (2012). Cytokinesis in trypanosomes. *Cytoskeleton* 69, 931–941.

Field, M. C. and Carrington, M. (2009). The trypanosome flagellar pocket. *Nat. Rev. Microbiol.* 7, 775–786.

Finn, R. D., Clements, J. and Eddy, S. R. (2011). HMMER web server: interactive sequence similarity searching. *Nucleic Acids Res.* 39, W29–W37.

Florimond, C., Sahin, A., Vidilaseris, K., Dong, G., Landrein, N., Dacheux, D., Albisetti, A., Byard, E. H., Bonhivers, M. and Robinson, D. R. (2015). BILBO1 Is a Scaffold Protein of the Flagellar Pocket Collar in the Pathogen Trypanosoma brucei. *PLOS Pathog.* 11, e1004654.

Gambarotto, D., Hamel, V. and Guichard, P. (2021). Ultrastructure expansion microscopy (U-ExM). *Methods Cell Biol.* 161, 57–81.

Garcia-Gonzalo, F. R. and Reiter, J. F. (2017). Open Sesame: How Transition Fibers and the Transition Zone Control Ciliary Composition. *Cold Spring Harb. Perspect. Biol.* 9, a028134.

Geimer, S. and Melkonian, M. (2004). The ultrastructure of the *Chlamydomonas reinhardtii* basal apparatus: identification of an early marker of radial asymmetry inherent in the basal body. *J. Cell Sci.* 117, 2663–2674.

Gheiratmand, L., Brasseur, A., Zhou, Q. and He, C. Y. (2013). Biochemical Characterization of the Bi-lobe Reveals a Continuous Structural Network Linking the Bi-lobe to Other Single-copied Organelles in *Trypanosoma brucei*. *J. Biol. Chem.* 288, 3489–3499.

Gonçalves, J. and Pelletier, L. (2017). The Ciliary Transition Zone: Finding the Pieces and Assembling the Gate. *Mol. Cells* 40, 243–253.

Gorilak, P., Pružincová, M., Vachova, H., Olšinová, M., Schmidt Cernohorska, M. and Varga, V. (2021). Expansion microscopy facilitates quantitative super-resolution studies of cytoskeletal structures in kinetoplastid parasites. *Open Biol.* 11, 210131.

Graser, S., Stierhof, Y.-D., Lavoie, S. B., Gassner, O. S., Lamla, S., Le Clech, M. and Nigg, E. A. (2007). Cep164, a novel centriole appendage protein required for primary cilium formation. *J. Cell Biol.* 179, 321–330.

Greenan, G. A., Vale, R. D. and Agard, D. A. (2020). Electron cryotomography of intact motile cilia defines the basal body to axoneme transition. *J. Cell Biol.* 219, e201907060.

Gull, K. (1999). The Cytoskeleton of Trypanosomatid Parasites. *Annu. Rev. Microbiol.* 53, 629–655.

Hall, N. A. and Hehnly, H. (2021). A centriole's subdistal appendages: contributions to cell division, ciliogenesis and differentiation. *Open Biol.* 11, 200399.

Hammarton, T. C., Clark, J., Douglas, F., Boshart, M. and Mottram, J. C. (2003). Stage-specific differences in cell cycle control in Trypanosoma brucei revealed by RNA interference of a mitotic cyclin. *J. Biol. Chem.* 278, 22877–22886.

Hannaert, V., Albert, M.-A., Rigden, D. J., Theresa da Silva Giotto, M., Thiemann, O., Garratt, R. C., Van Roy, J., Opperdoes, F. R. and Michels, P. A. M. (2003). Kinetic characterization, structure modelling studies and crystallization of Trypanosoma brucei enolase. *Eur. J. Biochem.* 270, 3205–3213.

Harmer, J., Qi, X., Toniolo, G., Patel, A., Shaw, H., Benson, F. E., Ginger, M. L. and McKean, P. G. (2017). Variation in Basal Body Localisation and Targeting of Trypanosome RP2 and FOR20 Proteins. *Protist* 168, 452–466.

Hatch, E. and Stearns, T. (2010). The Life Cycle of Centrioles. *Cold Spring Harb. Symp. Quant. Biol.* 75, 425–431.

Hilton, N. A., Sladewski, T. E., Perry, J. A., Pataki, Z., Sinclair-Davis, A. N., Muniz, R. S., Tran, H. L., Wurster, J. I., Seo, J. and de Graffenried, C. L. (2018). Identification of TOEFAZ1-interacting proteins reveals key regulators of Trypanosoma brucei cytokinesis. *Mol. Microbiol.* 109, 306–326.

Hiraki, M., Nakazawa, Y., Kamiya, R. and Hirono, M. (2007). Bld10p Constitutes the Cartwheel-Spoke Tip and Stabilizes the 9-Fold Symmetry of the Centriole. *Curr. Biol.* 17, 1778–1783.

Hodges, M. E., Scheumann, N., Wickstead, B., Langdale, J. A. and Gull, K. (2010). Reconstructing the evolutionary history of the centriole from protein components. *J. Cell Sci.* 123, 1407–1413.

Hughes, L., Towers, K., Starborg, T., Gull, K. and Vaughan, S. (2013). A cell-body groove housing the new flagellum tip suggests an adaptation of cellular morphogenesis for parasitism in the bloodstream form of Trypanosoma brucei. *J. Cell Sci.* 126, 5748–5757.

Hughes, L., Borrett, S., Towers, K., Starborg, T. and Vaughan, S. (2017). Patterns of organelle ontogeny through a cell cycle revealed by whole-cell reconstructions using 3D electron microscopy. *J. Cell Sci.* 130, 637–647.

Ikeda, K. N. and de Graffenried, C. L. (2012). Polo-like kinase is necessary for flagellum inheritance in *Trypanosoma brucei*. *J. Cell Sci.* jcs.101162.

Inoko, A., Yano, T., Miyamoto, T., Matsuura, S., Kiyono, T., Goshima, N., Inagaki, M. and Hayashi, Y. (2018). Albatross/FBF1 contributes to both centriole duplication and centrosome separation. *Genes Cells* 23, 1023–1042.

Isch, C., Majneri, P., Landrein, N., Pivovarova, Y., Lesigang, J., Lauruol, F., Robinson, D. R., Dong, G. and Bonhivers, M. (2021). Structural and functional studies of the first tripartite protein complex at the Trypanosoma brucei flagellar pocket collar. *PLOS Pathog.* 17, e1009329.

Jana, S. C., Marteil, G. and Bettencourt-Dias, M. (2014). Mapping molecules to structure: unveiling secrets of centriole and cilia assembly with near-atomic resolution. *Curr. Opin. Cell Biol.* 26, 96–106.

Jonsdottir, A. B., Dirks, R. W., Vrolijk, J., Ögmundsdottir, H. M., Tanke, H. J., Eyfjörd, J. E. and Szuhai, K. (2010). Centriole movements in mammalian epithelial cells during cytokinesis. *BMC Cell Biol.* 11, 34.

Joo, K., Kim, C. G., Lee, M.-S., Moon, H.-Y., Lee, S.-H., Kim, M. J., Kweon, H.-S., Park, W.-Y., Kim, C.-H., Gleeson, J. G., et al. (2013). CCDC41 is required for ciliary vesicle docking to the mother centriole. *Proc. Natl. Acad. Sci.* 110, 5987–5992.

Katoh, Y., Chiba, S. and Nakayama, K. (2020). Practical method for superresolution imaging of primary cilia and centrioles by expansion microscopy using an amplibody for fluorescence signal amplification. *Mol. Biol. Cell* 31, 2195–2206.

Kobayashi, T. and Dynlacht, B. D. (2011). Regulating the transition from centriole to basal body. *J. Cell Biol.* 193, 435–444.

Kohl, L., Sherwin, T. and Gull, K. (1999). Assembly of the paraflagellar rod and the flagellum attachment zone complex during the Trypanosoma brucei cell cycle. *J. Eukaryot. Microbiol.* 46, 105–109.

Kuhn, M., Hyman, A. A. and Beyer, A. (2014). Coiled-Coil Proteins Facilitated the Functional Expansion of the Centrosome. *PLoS Comput. Biol.* 10, e1003657.

Kumar, D. and Reiter, J. (2021). How the centriole builds its cilium: of mothers, daughters, and the acquisition of appendages. *Curr. Opin. Struct. Biol.* 66, 41–48.

Kumar, P. and Wang, C. C. (2005). Depletion of anaphase-promoting complex or cyclosome (APC/C) subunit homolog APC1 or CDC27 of Trypanosoma brucei arrests the procyclic form in metaphase but the bloodstream form in anaphase. *J. Biol. Chem.* 280, 31783–31791.

Kurasawa, Y., Hu, H., Zhou, Q. and Li, Z. (2018). The trypanosome-specific protein CIF3 cooperates with the CIF1 protein to promote cytokinesis in Trypanosoma brucei. *J. Biol. Chem.* 293, 10275–10286.

Kurasawa, Y., Lee, K. J. and Li, Z. (2022). Structural Domains of CIF3 Required for Interaction with Cytokinesis Regulatory Proteins and for Cytokinesis Initiation in Trypanosoma brucei. *mSphere* e00047-22.

Lacomble, S., Vaughan, S., Gadelha, C., Morphew, M. K., Shaw, M. K., McIntosh, J. R. and Gull, K. (2009). Three-dimensional cellular architecture of the flagellar pocket and associated cytoskeleton in trypanosomes revealed by electron microscope tomography. *J. Cell Sci.* 122, 1081–1090.

Lacomble, S., Vaughan, S., Gadelha, C., Morphew, M. K., Shaw, M. K., McIntosh, J. R. and Gull, K. (2010). Basal body movements orchestrate membrane organelle division and cell morphogenesis in Trypanosoma brucei. *J. Cell Sci.* 123, 2884–2891.

LaCount, D. J., Barrett, B. and Donelson, J. E. (2002). Trypanosoma brucei FLA1 Is Required for Flagellum Attachment and Cytokinesis*. *J. Biol. Chem.* 277, 17580–17588.

Lai, D.-H., Moreira-Leite, F., Xu, Z.-S., Yang, J. and Gull, K. (2021). A specific basal body linker protein provides the connection function for basal body inheritance in trypanosomes. *Proc. Natl. Acad. Sci.* 118,.

Langousis, G. and Hill, K. L. (2014). Motility and more: the flagellum of Trypanosoma brucei. *Nat. Rev. Microbiol.* 12, 505–518.

Lemos, M., Mallet, A., Bertiaux, E., Imbert, A., Rotureau, B. and Bastin, P. (2020). Timing and original features of flagellum assembly in trypanosomes during development in the tsetse fly. *Parasit. Vectors* 13, 169.

Madeira, F., Park, Y. M., Lee, J., Buso, N., Gur, T., Madhusoodanan, N., Basutkar, P., Tivey, A. R. N., Potter, S. C., Finn, R. D., et al. (2019). The EMBL-EBI search and sequence analysis tools APIs in 2019. *Nucleic Acids Res.* 47, W636–W641.

Matsuura, K., Lefebvre, P. A., Kamiya, R. and Hirono, M. (2004). Bld10p, a novel protein essential for basal body assembly in Chlamydomonas. *J. Cell Biol.* 165, 663–671.

Matthews, K. R. (1999). Developments in the Differentiation of Trypanosoma brucei. *Parasitol. Today* 15, 76–80.

McAllaster, M. R., Ikeda, K. N., Lozano-Núñez, A., Anrather, D., Unterwurzacher, V., Gossenreiter, T., Perry, J. A., Crickley, R., Mercadante, C. J., Vaughan, S., et al. (2015). Proteomic identification of novel cytoskeletal proteins associated with TbPLK, an essential regulator of cell morphogenesis in Trypanosoma brucei. *Mol. Biol. Cell* 26, 3013–3029.

Melville, S. E., Leech, V., Navarro, M. and Cross, G. A. M. (2000). The molecular karyotype of the megabase chromosomes of Trypanosoma brucei stock 427. *Mol. Biochem. Parasitol.* 111, 261–273.

Mennella, V., Keszthelyi, B., McDonald, K. L., Chhun, B., Kan, F., Rogers, G. C., Huang, B. and Agard, D. A. (2012). Subdiffraction-resolution fluorescence microscopy reveals a domain of the centrosome critical for pericentriolar material organization. *Nat. Cell Biol.* 14, 1159–1168.

Morga, B. and Bastin, P. (2013). Getting to the heart of intraflagellar transport using Trypanosoma and Chlamydomonas models: the strength is in their differences. *Cilia* 2, 16.

Morgan, G. W., Denny, P. W., Vaughan, S., Goulding, D., Jeffries, T. R., Smith, D. F., Gull, K. and Field, M. C. (2005). An Evolutionarily Conserved Coiled-Coil Protein Implicated in Polycystic Kidney Disease Is Involved in Basal Body Duplication and Flagellar Biogenesis in *Trypanosoma brucei*. *Mol. Cell. Biol.* 25, 3774–3783.

Morriswood, B., He, C. Y., Sealey-Cardona, M., Yelinek, J., Pypaert, M. and Warren, G. (2009). The bilobe structure of Trypanosoma brucei contains a MORN-repeat protein. *Mol. Biochem. Parasitol.* 167, 95–103.

Nachury, M. V. (2018). The molecular machines that traffic signaling receptors into and out of cilia. *Curr. Opin. Cell Biol.* 51, 124–131.

Ogbadoyi, E. O., Robinson, D. R. and Gull, K. (2003). A High-Order *Trans* -Membrane Structural Linkage Is Responsible for Mitochondrial Genome Positioning and Segregation by Flagellar Basal Bodies in Trypanosomes. *Mol. Biol. Cell* 14, 1769–1779.

O'Toole, E. T., Giddings, T. H., McIntosh, J. R. and Dutcher, S. K. (2003). Three-dimensional Organization of Basal Bodies from Wild-Type and δ-Tubulin Deletion Strains of *Chlamydomonas reinhardtii*. *Mol. Biol. Cell* 14, 2999–3012.

Overath, P. and Engstler, M. (2004). Endocytosis, membrane recycling and sorting of GPI-anchored proteins: Trypanosoma brucei as a model system: The endocytic system of T. brucei. *Mol. Microbiol.* 53, 735–744.

Paintrand, M., Moudjou, M., Delacroix, H. and Bornens, M. (1992). Centrosome organization and centriole architecture: Their sensitivity to divalent cations. *J. Struct. Biol.* 108, 107–128.

Pearson, C. G. (2014). Choosing sides--asymmetric centriole and basal body assembly. *J. Cell Sci.* 127, 2803–2810.

Perdomo, D., Berdance, E., Lallinger-Kube, G., Sahin, A., Dacheux, D., Landrein, N., Cayrel, A., Ersfeld, K., Bonhivers, M., Kohl, L., et al. (2022). TbKINX1B: a novel BILBO1 partner and an essential protein in bloodstream form *Trypanosoma brucei*. *Parasite* 29, 14.

Piel, M., Nordberg, J., Euteneuer, U. and Bornens, M. (2001). Centrosome-Dependent Exit of Cytokinesis in Animal Cells. *Science* 291, 1550–1553.

Poon, S. K., Peacock, L., Gibson, W., Gull, K. and Kelly, S. (2012). A modular and optimized single marker system for generating Trypanosoma brucei cell lines expressing T7 RNA polymerase and the tetracycline repressor. *Open Biol.* 2, 110037.

Pradel, L. C., Bonhivers, M., Landrein, N. and Robinson, D. R. (2006). NIMA-related kinase *Tb* NRKC is involved in basal body separation in *Trypanosoma brucei*. *J. Cell Sci.* 119, 1852–1863.

Ralston, K. S., Lerner, A. G., Diener, D. R. and Hill, K. L. (2006). Flagellar motility contributes to cytokinesis in Trypanosoma brucei and is modulated by an evolutionarily conserved dynein regulatory system. *Eukaryot. Cell* 5, 696–711.

Reiter, J. F., Blacque, O. E. and Leroux, M. R. (2012). The base of the cilium: roles for transition fibres and the transition zone in ciliary formation, maintenance and compartmentalization. *EMBO Rep.* 13, 608–618.

Robinson, D. R., Sherwin, T., Ploubidou, A., Byard, E. H. and Gull, K. (1995). Microtubule polarity and dynamics in the control of organelle positioning, segregation, and cytokinesis in the trypanosome cell cycle. *J. Cell Biol.* 128, 1163–1172.

Schneider, C. A., Rasband, W. S. and Eliceiri, K. W. (2012). NIH Image to ImageJ: 25 years of image analysis. *Nat. Methods* 9, 671–675.

Schumann Burkard, G., Jutzi, P. and Roditi, I. (2011). Genome-wide RNAi screens in bloodstream form trypanosomes identify drug transporters. *Mol. Biochem. Parasitol.* 175, 91–94.

Sherwin, T., Gull, K. and Vickerman, K. (1989). The cell division cycle of Trypanosoma brucei brucei: timing of event markers and cytoskeletal modulations. *Philos. Trans. R. Soc. Lond. B Biol. Sci.* 323, 573–588.

Sinclair, A. N. and de Graffenried, C. L. (2019). More than Microtubules: The Structure and Function of the Subpellicular Array in Trypanosomatids. *Trends Parasitol.* 35, 760–777.

Sinclair-Davis, A. N., McAllaster, M. R. and de Graffenried, C. L. (2017). A functional analysis of TOEFAZ1 uncovers protein domains essential for cytokinesis in *Trypanosoma brucei*. *J. Cell Sci.* 130, 3918–3932.

Slaats, G. G., Ghosh, A. K., Falke, L. L., Le Corre, S., Shaltiel, I. A., van de Hoek, G., Klasson, T. D., Stokman, M. F., Logister, I., Verhaar, M. C., et al. (2014). Nephronophthisis-Associated CEP164 Regulates Cell Cycle Progression, Apoptosis and Epithelial-to-Mesenchymal Transition. *PLoS Genet.* 10, e1004594.

Stephan, A., Vaughan, S., Shaw, M. K., Gull, K. and McKean, P. G. (2007). An Essential Quality Control Mechanism at the Eukaryotic Basal Body Prior to Intraflagellar Transport. *Traffic* 8, 1323–1330.

Steverding, D. (2008). The history of African trypanosomiasis. *Parasit. Vectors* 1, 3.

Sunter, J. D. and Gull, K. (2016). The Flagellum Attachment Zone: 'The Cellular Ruler' of Trypanosome Morphology. *Trends Parasitol.* 32, 309–324.

Tanos, B. E., Yang, H.-J., Soni, R., Wang, W.-J., Macaluso, F. P., Asara, J. M. and Tsou, M.-F. B. (2013). Centriole distal appendages promote membrane docking, leading to cilia initiation. *Genes Dev.* 27, 163–168.

Taylor, A. E. and Godfrey, D. G. (1969). A new organelle of bloodstream salivarian trypanosomes. *J. Protozool.* 16, 466–470.

Tischer, J., Carden, S. and Gergely, F. (2021). Accessorizing the centrosome: new insights into centriolar appendages and satellites. *Curr. Opin. Struct. Biol.* 66, 148–155.

Trépout, S., Tassin, A.-M., Marco, S. and Bastin, P. (2018). STEM tomography analysis of the trypanosome transition zone. *J. Struct. Biol.* 202, 51–60.

Tyler, K. (2001). Anisomorphic Cell Division by African Trypanosomes. *Protist* 152, 367–378.

Uversky, V. N. (2013). Under-folded proteins: Conformational ensembles and their roles in protein folding, function, and pathogenesis: Under-Folded Proteins. *Biopolymers* 99, 870–887.

Uzbekov, R. and Alieva, I. (2018). Who are you, subdistal appendages of centriole? *Open Biol.* 8, 180062.

Varga, V., Moreira-Leite, F., Portman, N. and Gull, K. (2017). Protein diversity in discrete structures at the distal tip of the trypanosome flagellum. *Proc. Natl. Acad. Sci. U. S. A.* 114, E6546–E6555.

Vaughan, S. and Gull, K. (2016). Basal body structure and cell cycle-dependent biogenesis in Trypanosoma brucei. *Cilia* 5,.

Vickerman, K. (1962). The mechanism of cyclical development in trypanosomes of the Trypanosoma brucei sub-group: An hypothesis based on ultrastructural observations. *Trans. R. Soc. Trop. Med. Hyg.* 56, 487–495.

Wei, Q., Xu, Q., Zhang, Y., Li, Y., Zhang, Q., Hu, Z., Harris, P. C., Torres, V. E., Ling, K. and Hu, J. (2013). Transition fibre protein FBF1 is required for the ciliary entry of assembled intraflagellar transport complexes. *Nat. Commun.* 4, 2750.

Wei, Q., Ling, K. and Hu, J. (2015). The essential roles of transition fibers in the context of cilia. *Curr. Opin. Cell Biol.* 35, 98–105.

Wheeler, R. J., Scheumann, N., Wickstead, B., Gull, K. and Vaughan, S. (2013). Cytokinesis in Trypanosoma brucei differs between bloodstream and tsetse trypomastigote forms: implications for microtubule-based morphogenesis and mutant analysis. *Mol. Microbiol.* 90, 1339–1355.

Wheeler, R. J., Gull, K. and Sunter, J. D. (2019). Coordination of the Cell Cycle in Trypanosomes. *Annu. Rev. Microbiol.* 73, 133–154.

Willcox, C. R., Pitard, V., Netzer, S., Couzi, L., Salim, M., Silberzahn, T., Moreau, J.-F., Hayday, A. C., Willcox, B. E. and Déchanet-Merville, J. (2012). Cytomegalovirus and tumor stress surveillance by binding of a human γδ T cell antigen receptor to endothelial protein C receptor. *Nat. Immunol.* 13, 872–879.

Winey, M. and O'Toole, E. (2014). Centriole structure. *Philos. Trans. R. Soc. B Biol. Sci.* 369, 20130457.

Wirtz, E., Leal, S., Ochatt, C. and Cross, GeorgeA. M. (1999). A tightly regulated inducible expression system for conditional gene knock-outs and dominant-negative genetics in Trypanosoma brucei. *Mol. Biochem. Parasitol.* 99, 89–101.

Woods, A., Sherwin, T., Sasse, R., MacRae, T. H., Baines, A. J. and Gull, K. (1989). Definition of individual components within the cytoskeleton of Trypanosoma brucei by a library of monoclonal antibodies. *J. Cell Sci.* 93 (Pt 3), 491–500.

Yang, T. T., Chong, W. M., Wang, W.-J., Mazo, G., Tanos, B., Chen, Z., Tran, T. M. N., Chen, Y.-D., Weng, R. R., Huang, C.-E., et al. (2018). Super-resolution architecture of mammalian centriole distal appendages reveals distinct blade and matrix functional components. *Nat. Commun.* 9, 2023.

Zhang, X., An, T., Pham, K. T. M., Lun, Z.-R. and Li, Z. (2019). Functional Analyses of Cytokinesis Regulators in Bloodstream Stage Trypanosoma brucei Parasites Identify Functions and Regulations Specific to the Life Cycle Stage. *mSphere* 4,.

Zhou, Q. and Li, Z. (2016). A backup cytokinesis pathway in *Trypanosoma brucei*. *Cell Cycle* 15, 2379–2380.

Zhou, Q., Gu, J., Lun, Z.-R., Ayala, F. J. and Li, Z. (2016a). Two distinct cytokinesis pathways drive trypanosome cell division initiation from opposite cell ends. *Proc. Natl. Acad. Sci. U. S. A.* 113, 3287–3292.

Zhou, Q., Hu, H. and Li, Z. (2016b). An EF-hand-containing Protein in Trypanosoma brucei Regulates Cytokinesis Initiation by Maintaining the Stability of the Cytokinesis Initiation Factor CIF1. *J. Biol. Chem.* 291, 14395–14409.

Zhou, Q., An, T., Pham, K. T. M., Hu, H. and Li, Z. (2018). The CIF1 protein is a master orchestrator of trypanosome cytokinesis that recruits several cytokinesis regulators to the cytokinesis initiation site. *J. Biol. Chem.* 293, 16177–16192.

Figures

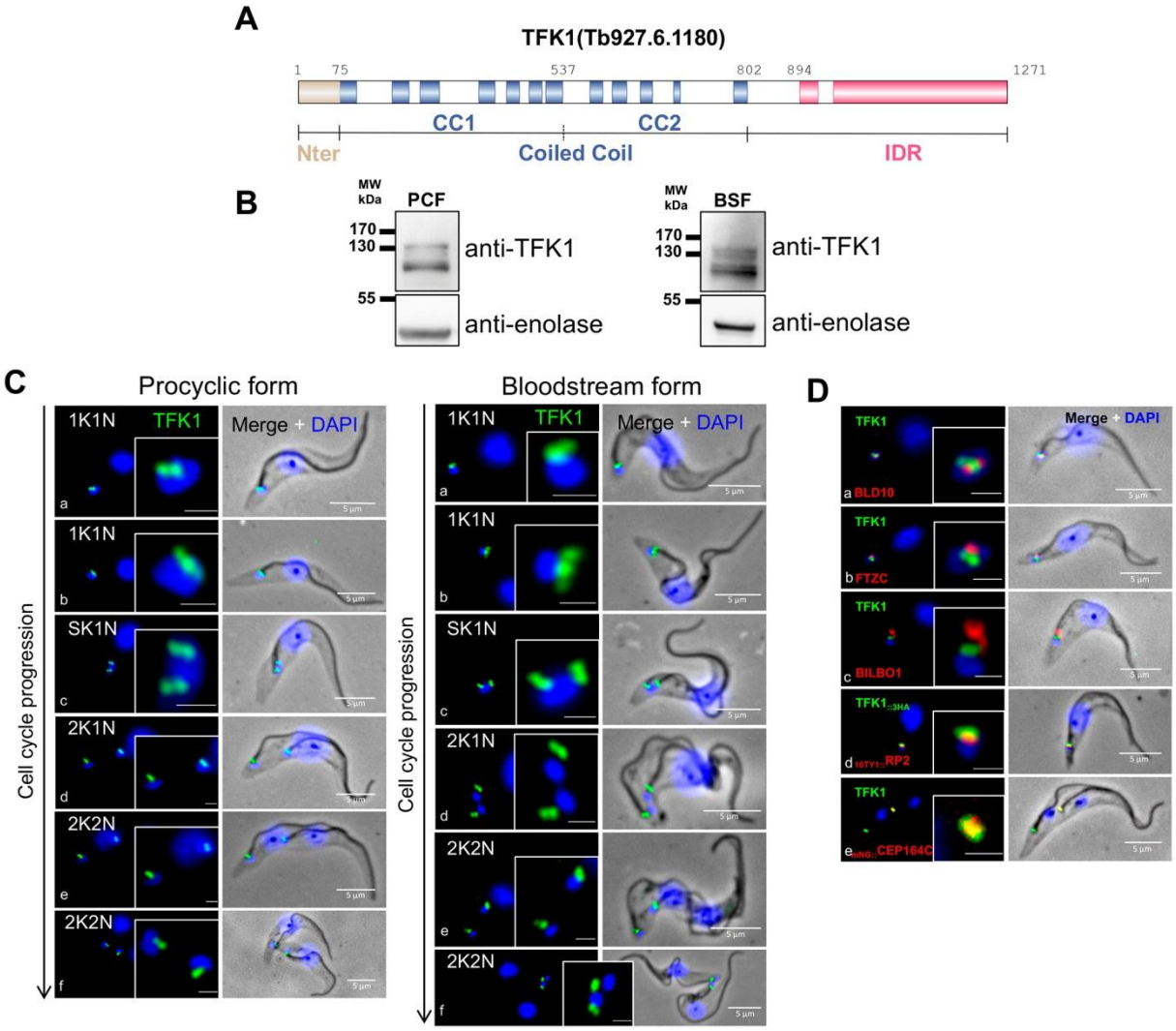

Fig. 1: TFK1 (Tb927.6.1180) is a coiled-coil protein localized at the basal body region

(A) Representation of TFK1 domains composed of a N-terminal region (aa 1-74), a central coiled-coil region (aa 75-802) composed by twelve coiled-coil protein domains divided into CC1 (aa 75-536) and CC2 (aa 537-802) and a C-terminal intrinsically disordered region (IDR) (aa 803-1271). (B) Western blots of TFK1 using anti-TFK1 in PCF and BSF wild-type whole cells (enolase as loading charge). (C) Immunofluorescence labeling on detergent-extracted cells of TFK1 (green, anti-TFK1) across the cell cycle in PCF and BSF forms. (D)

Immunofluorescence on detergent-extracted cells showing the co-localization of TFK1 (green, anti-TFK1) with BLD10 (red, basal body marker) (a), FTZC (red, transition zone marker) (b), BILBO1 (red, flagellar pocket collar marker) (c), endogenously tagged $_{TY1::}$RP2 (red) (d) and $_{mNeonGreen::}$CEP164C (red) (e). Scale bars: 5 µm, inset 1 µm.

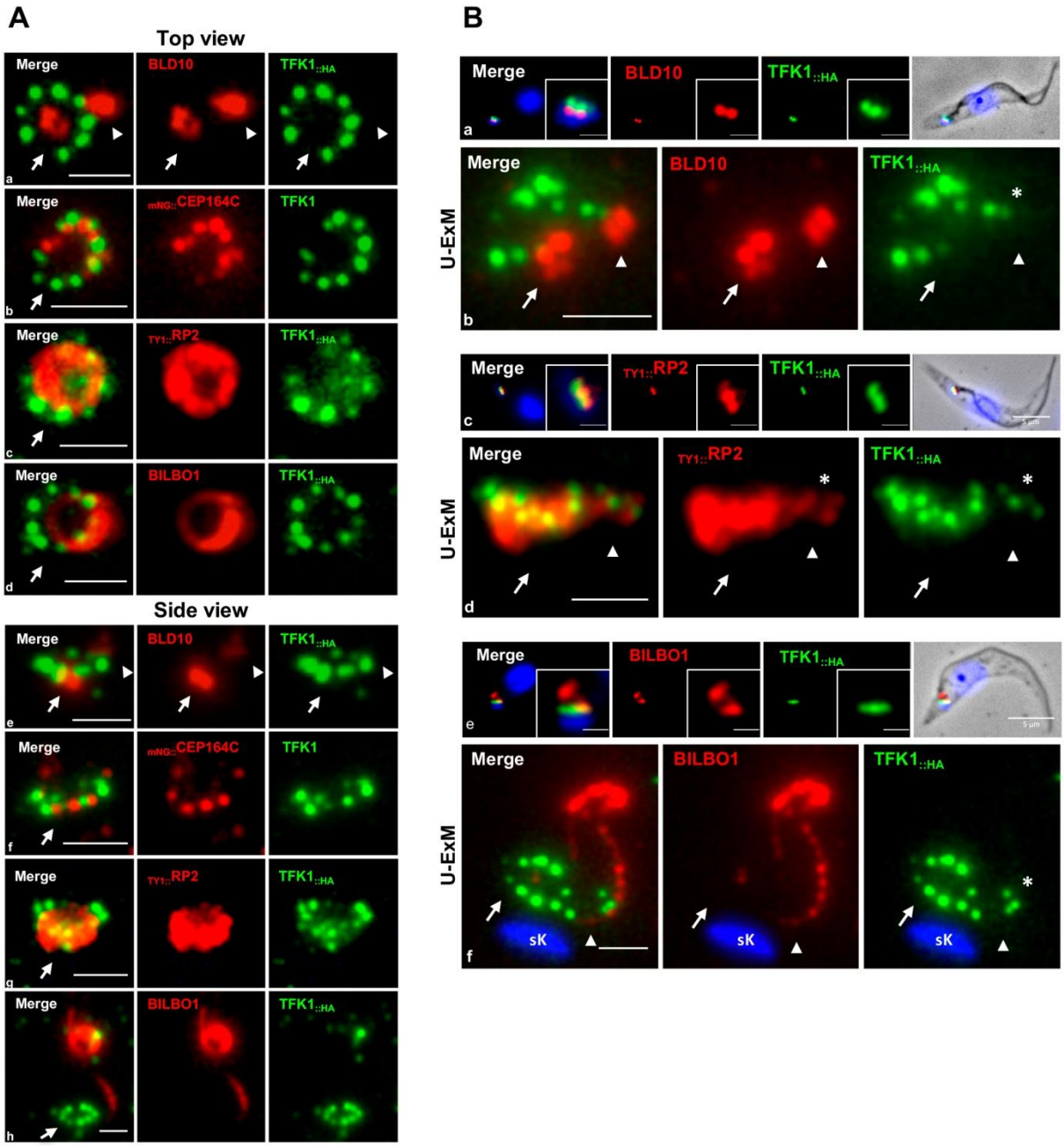

Fig. 2: TFK1, a newly identified transition fibres protein and a marker of basal body maturation

(A) Top (a-d) and side (e-h) views of Ultrastructure Expansion Microscopy (U-ExM) showing the co-labelling of TFK1 using anti-TFK1 in endogenously tagged TFK1$_{::HA}$ background PCF whole cells (green), and of BLD10 (red) (a), of $_{mNG::}$CEP164C (red) (b), of $_{TY1::}$RP2 (red) (c) and of BILBO1 (red) (d) in G1 stage cells. (B) Immunofluorescence (a, c, e) and U-ExM (b,

d, f) on detergent-extracted cells showing the co-labelling of endotagged TFK1$_{::HA}$ (green) and BLD10 (red) (a, b), endotagged TFK1$_{::HA}$ (green) and endotagged $_{TY1::}$RP2 (red) (c, d), endotagged TFK1$_{::HA}$ (green) and BILBO1 (red) during pro-BB maturation in SK1N cells stage (Early kinetoplast S phase) (e, f). The labeling on BB and pro-BB is indicated by an arrow and arrowhead respectively, and the maturing pro-BB by an asterisk. U-ExM pictures (Ae - f and Bb, d) are oriented with the kinetoplast downwards. Scale bars: (A) 5 µm, inset 1 µm and (B) 2 µm. Expansion factor: 4.8 fold.

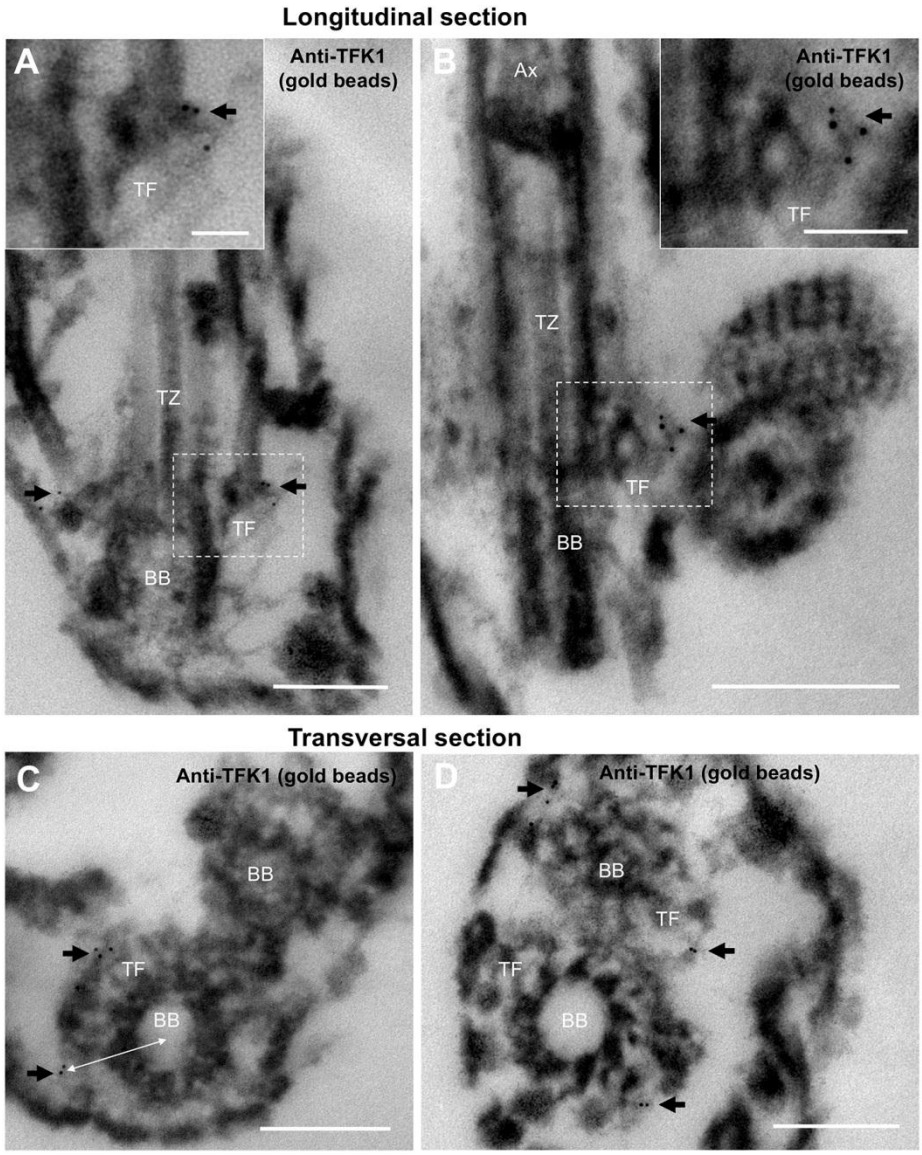

Fig. 3: TFK1 is localized at the tip of the transition fibres

Immuno-gold labeling on thin section of PCF whole cells showing the localization of TFK1 using anti-TFK1 (gold beads: black arrow). In A and B, views of longitudinal section of the mature basal body. In C and D, views of transversal sections of the basal bodies. BB: basal body, TF: transition fibres, TZ: transition zone, Ax: axoneme. The white double-arrow in C indicates measurements of the distance of TFK1 to the center of the basal body. Scale bars: 200 nm, insert 100 nm.

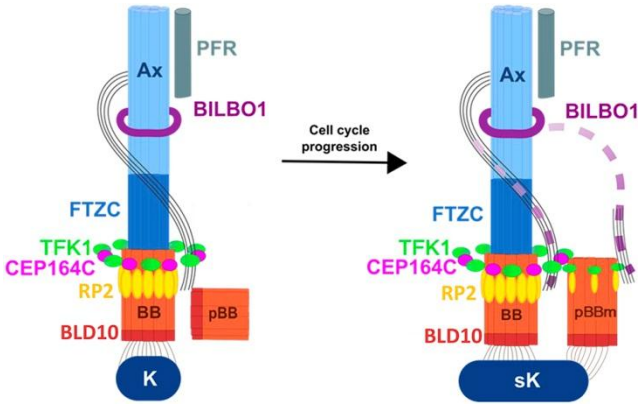

Fig. 4: Schematic representation of the subcellular localization of TFK1 together with key basal body markers in *Trypanosoma brucei*

Schematic representation showing the proposed model of TFK1 position in G1 stage (left scheme) and during the basal body maturation stage (right scheme). Ax: axoneme; PFR: paraflagellar rod; BILBO1 (Flagellar pocket marker); FTZC (transition zone marker); RP2 and CEP164C (transition fibres markers); BLD10 (BBs marker); BB: basal body, pBB: pro-basal body, pBBm: pro-BB maturation; K: kinetoplast and sK: kinetoplast in S phase.

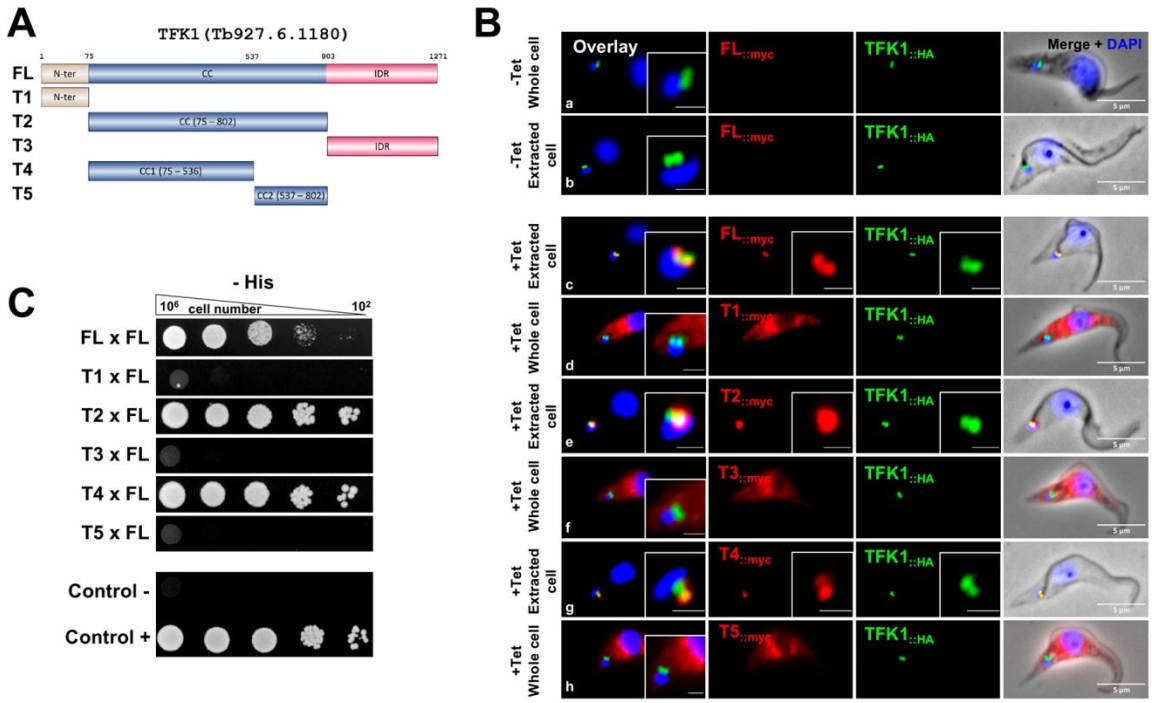

Fig. 5: Domain analysis of TFK1 shows key features

(A) Schematic representation of full length TFK1 (FL) and truncations (T1 N-ter aa 1-74; T2 CC aa 75-802; T3 IDR aa 803-1271; T4 CC1 aa 75-536; T5 CC2 aa 537-802). (B) Immunofluorescence labeling of $TFK1_{::myc}$ (red) in non-induced (a) and induced cells (b) and of truncations ($T1_{::myc}$, $T2_{::myc}$, $T3_{::myc}$, $T4_{::myc}$ and $T5_{::myc}$) (red) after 24 h of induction of expression in endogenously tagged $TFK1_{::HA}$ background (green) PCF cells Scale bars: 5 µm, insets 1 µm. (C) Yeast-two-hybrid assays on – Histidine selective medium (-His) of full-length TFK1 and truncated forms of TFK1. The negative control (Control -) was Lamin and T-antigen, and the positive control (Control +) was p53 and T-antigen.

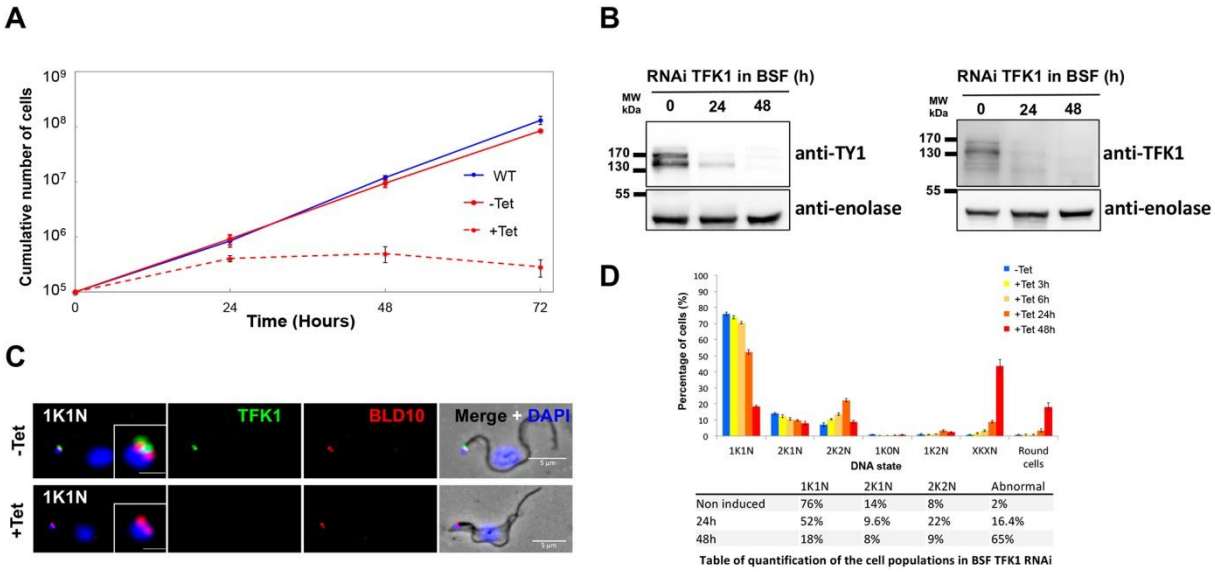

	1K1N	2K1N	2K2N	Abnormal
Non induced	76%	14%	8%	2%
24h	52%	9.6%	22%	16.4%
48h	18%	8%	9%	65%

Fig. 6: TFK1 is essential in bloodstream forms

(A) Growth curves of WT cells (blue line), non-induced cells (-Tet, red line) and tetracycline induced cells (+Tet, dashed red line) for TFK1 RNAi knockdown in BSF. (B) Representative western-blot analysis of the TFK1 protein level in endogenously tagged $_{TY1::}$TFK1 BSF using anti-TY1 (left blot) and anti-TFK1 (right blot) before induction and 24 and 48 h post induction. The anti-enolase was used as loading control. (C) Immunofluorescence on detergent-extracted PCF cells showing TFK1 (green) and BLD10 (red) before (-Tet) and 24 hours post induction +Tet); Scale bars: 5 µm, inset 1 µm. (D) Histogram of the nuclear and kinetoplast DNA content before the RNAi knockdown of TFK1 (-Tet) and 3 h, 6 h, 24 h and 48 h post induction induced in BSF TFK1 RNAi and table of quantification of the cell populations (abnormal cells including 1K2N, XKXN and round cells). (n>200, error bars: three independent experiments).

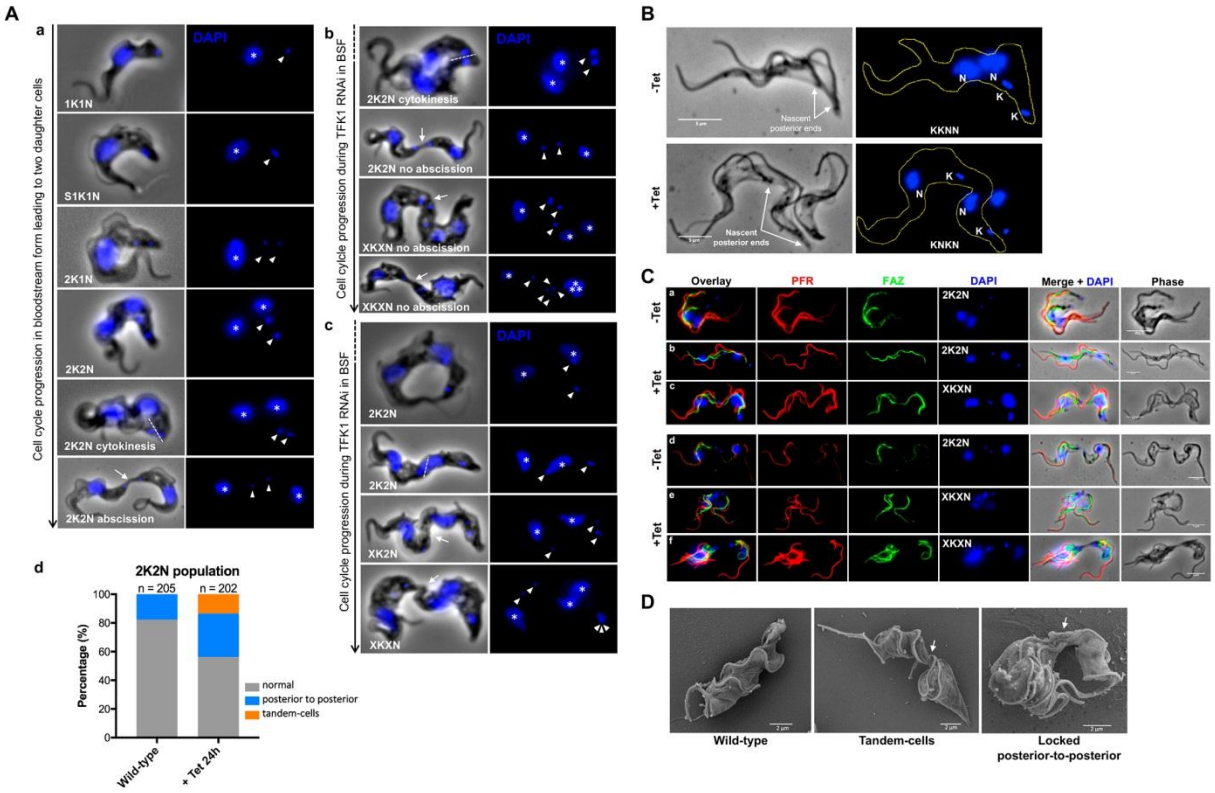

Fig. 7: TFK1 knockdown in BSF leads to cytokinesis defects

(A) DAPI staining on whole cells before (a) and after TFK1 RNAi knockdown (b and c) showing cell cycle progression (position of division fold generation, dashed line; nucleus (asterisk); kinetoplast (arrowhead); fold (dashed line); cytoplasmic bridge (arrow)). (d) Quantification of the 2K2N cell populations in wild-type population and in 24 h post induction of TFK1 RNAi knockdown population. normal stage (grey bar), cells in pre-abscission stage in "posterior-to-posterior" organization (blue bar) and "tandem-cells" forming abnormal KNKN organization (orange bar). (B) Detergent-extracted cytoskeleton cells preparation coupled with DAPI staining before (-Tet) and 24 h after (+Tet) TFK1 RNAi knockdown. (C) Immunofluorescence on detergent-extracted cells showing FAZ (flagellar attachment zone, green) and PFR (paraflagellar rod, red) labelling before (-Tet) and 24 h post induction (+Tet) that leads to the tandem-cells phenotype (b, c) and the cells locked posterior-to-posterior phenotype (e, f). Scale bars: 5 µm. (D) SEM analysis showing 2K2N wild-type cell (left) and TFK1 RNAi phenotypes after 24 h induction, tandem-cells (center) and cells in locked posterior-to-posterior organization (right). The arrows indicate the cytoplasmic bridge.

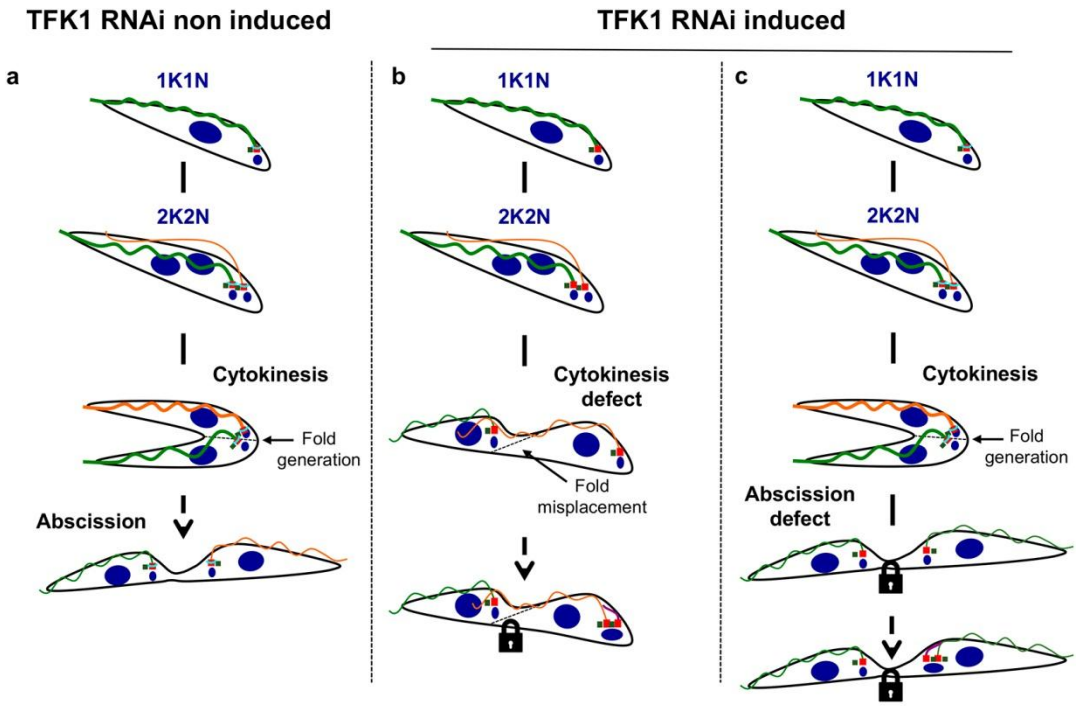

Index: TFK1 (cyan), old flagellum (green), new flagellum (orange), supernumerary flagellum (purple), basal body (red), pro-basal body (brown), nuclei and kinetoplasts (blue), final abscission defect (padlock)

Fig. 8: Schematic representation of the TFK1 knockdown leading to a deregulation of the cell division

(a) Representation of a normal cell cycle division in BSF cells, whereas (b) and (c) show abnormal division leading respectively to "tandem-cells" and "locked posterior-to-posterior" cells phenotypes.

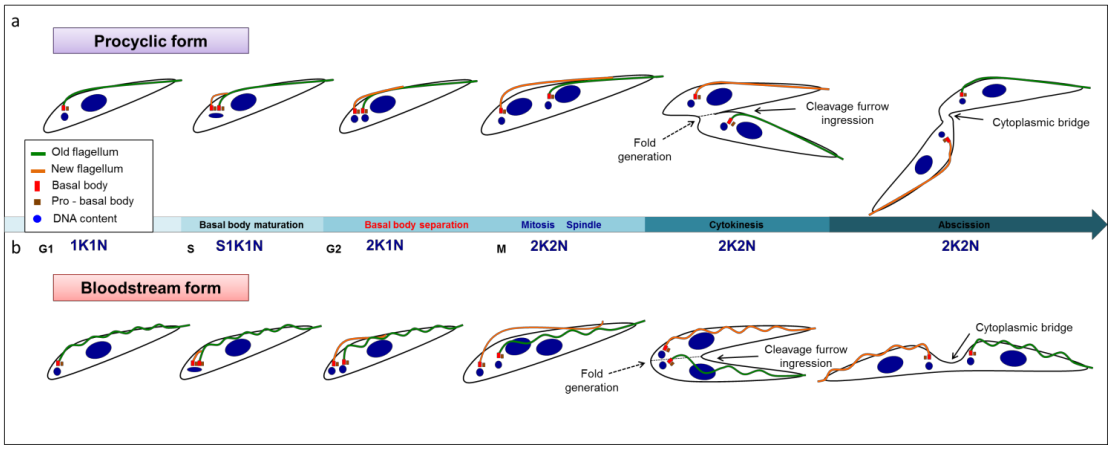

Fig. S1. *Trypanosoma brucei* shows differences in cell division according to the form Schematic representation of cell cycle in *Trypanosoma brucei*. a. The cell cycle in the insect stage procyclic form. b. The cell cycle in the mammalian bloodstream form.

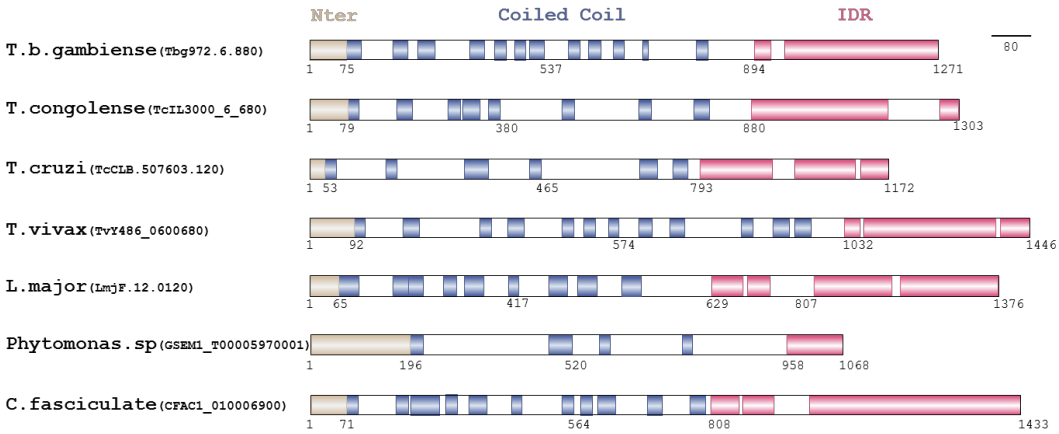

Fig. S2. TFK1 (Tb927.6.1180) is a coiled-coil kinetoplastid-specific protein

TFK1 protein orthologs of the class Kinetoplastida are aligned using ClustalW program (Madeira et al., 2019) and protein domains predicted by InterPro (Blum et al., 2021) are indicated with colored boxes: N-terminal region (Nter, brown boxes), coiled-coil domains (CC, blue boxes) and C-terminal intrinsically disordered region (IDR, pink boxes). The gene accession numbers encoding the putative proteins are indicated in parentheses.

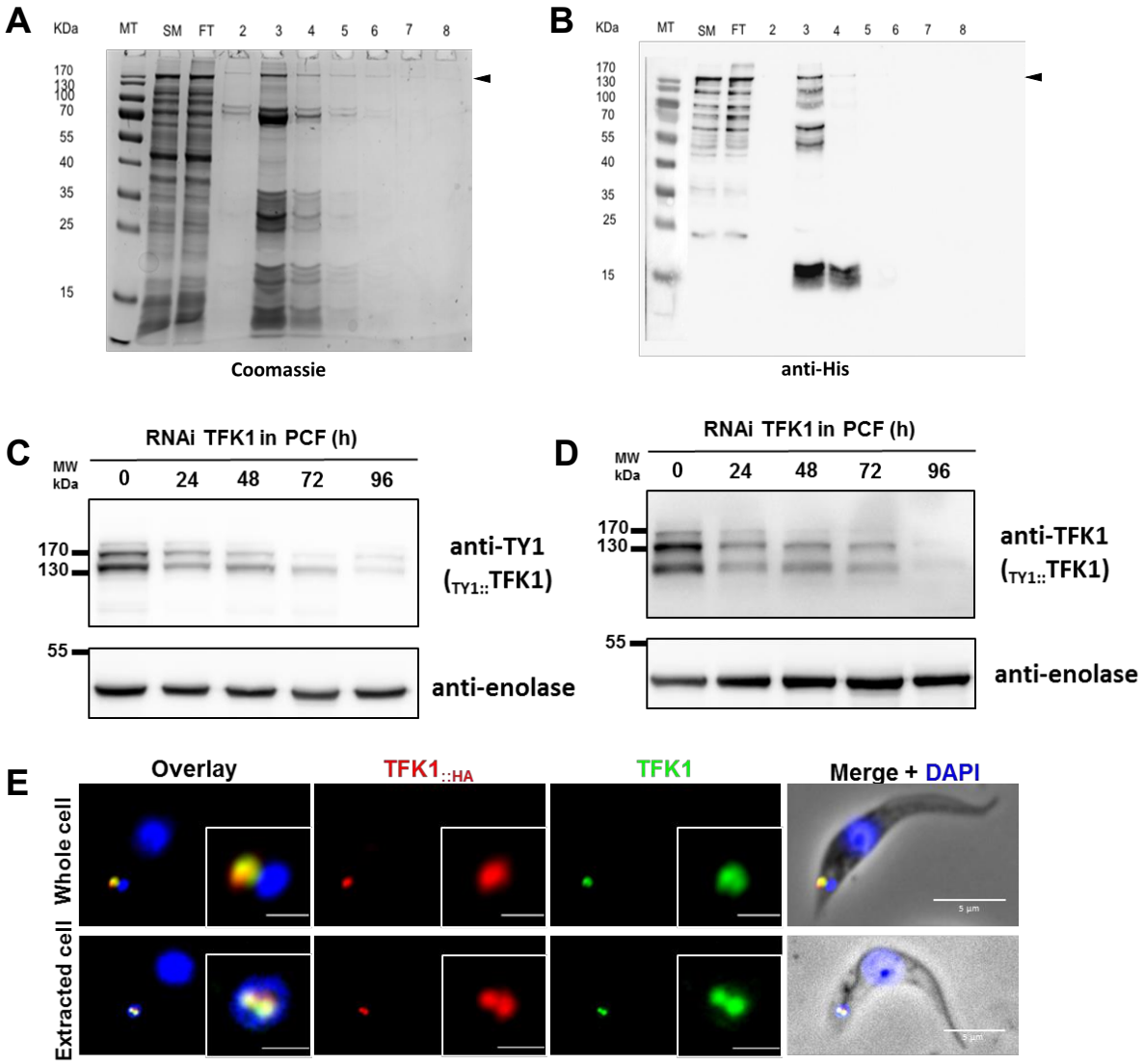

Fig. S3. Validation of the monoclonal antibody directed against TFK1 (anti-TFK1)

(A) Bacterial purified TFK1$_{::6His}$ (142 kDa indicated with black arrow heads) samples (SM: starting material, FT: flow through, 2-8: elutions) visualized by Coomasie blue staining and (B) by western blot using anti-His antibody. (C) and (D) western blots to monitor the protein level of TFK1 in endogenously tagged $_{TY1::}$TFK1 PCF (152.7 kDa) using both anti-TY1 and anti-TFK1 antibodies, respectively, before induction and 24 to 96 h post induction. (E) Immunofluorescence on detergent extracted (top panel) and whole cells (bottom panel) PCF showing the co-localization of TFK1 (green, anti-TFK1) and the endogenously tagged TFK1$_{::HA}$ (red, anti-HA antibody). Scale bar: 5 µm, inset 1 µm.

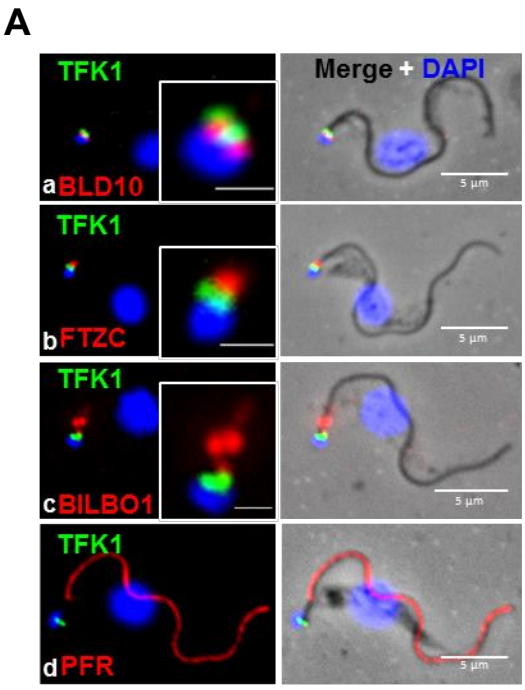

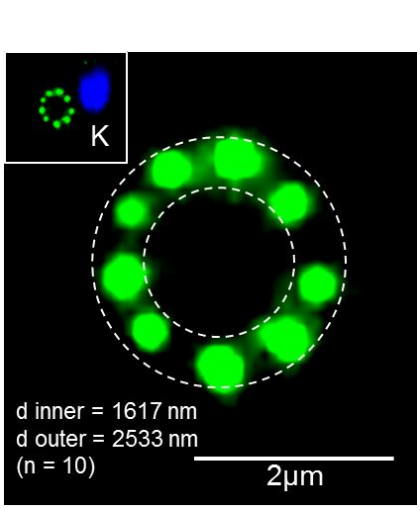

Ultrastructure expansion microscopy TFK1 diameter (nm)

Post-expansion		Expansion factor	Calculated		
Inner	Outer		Inner	Outer	
1597.3	2550.3	4.5	354.9	566.7	
1506.5	2470.4	4	376.6	617.6	
1570.2	2512.3	4.8	327.1	523.4	
1661	2661	4.8	346	554.3	
1699	2841.2	4.8	353.9	591.9	
1872.7	3036.2	4.5	416.1	674.7	
1593.4	2214.5	4.5	354.1	492.1	
1457.8	2253	4.5	323.9	500.6	
1497.7	2319.2	4.5	332.9	515.3	
1720.9	2471.5	4.5	382.8	549.2	
1617.6	2533		**356.8**	**558.6**	mean (nm)
124.6	257.8		28.3	56.8	s.d.

Fig. S4. **TFK1 localizes to the distal region of basal bodes with a nine-dotted circular pattern**

(A) Immunofluorescence on detergent-extracted BSF cells showing the co-localization of TFK1 (green, anti-TFK1) and BLD10 (red, BB marker), FTZC (red, transition zone marker), BILBO1 (red, flagellar pocket collar marker) and PFR (red, paraflagellar rod). Scale bars: 5 µm, inset 1 µm. (B) Top view of U-ExM experiments showing the labelling of TFK1 (green, anti-TFK1) composed of nine dots signal. The inner and outer diameters of the circular pattern indicated by the dashed circles were calculated from the measured distance (diameter)/expansion factor. The expansion factor is the ratio of the gel diameter after and before the expansion presented in the table (n=10). s.d.: standard deviation, K: kinetoplast, d: diameter, scale bars: 2 µm.

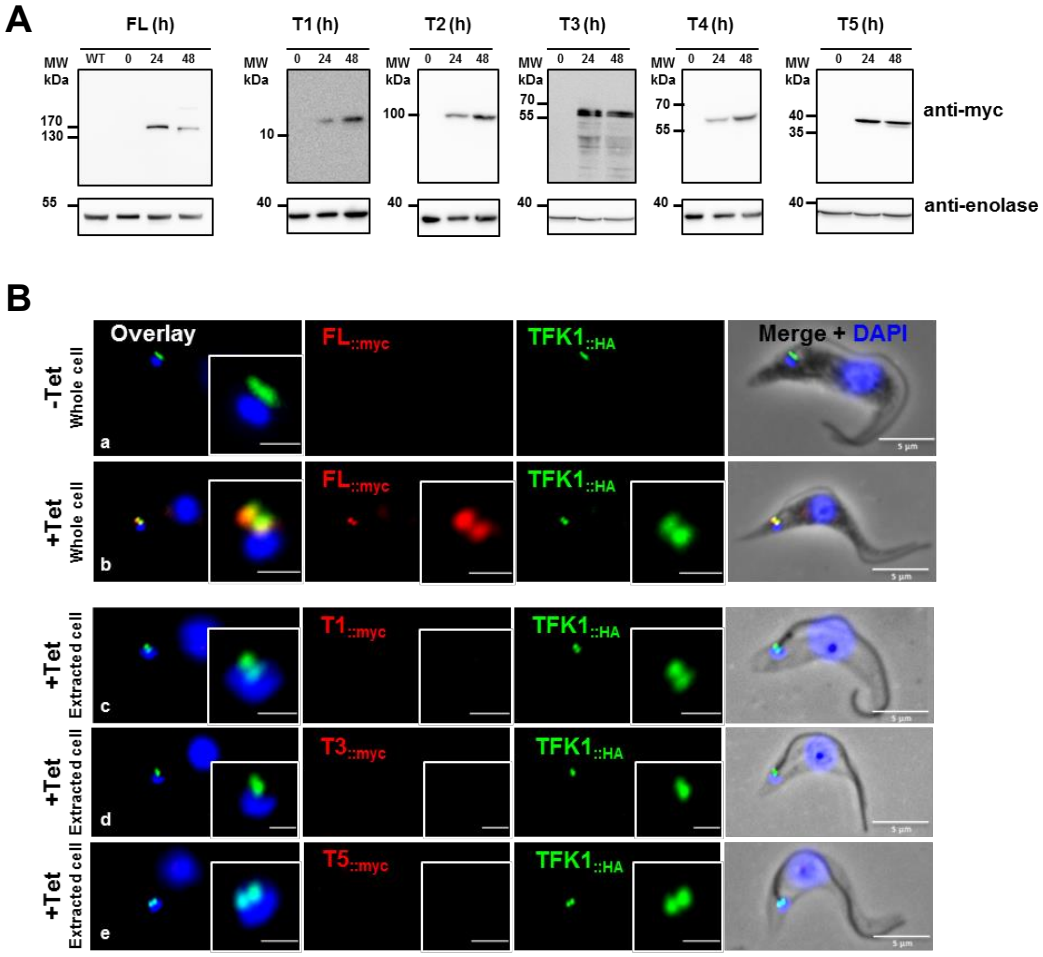

Fig. S5. Localization of ectopic expression and domains analysis of TFK1

(A) Western blot analysis after 24 h and 48 h induction of expression of FL TFK1$_{::myc}$ and truncations T1$_{::myc}$ (11.9 kDa), T2$_{::myc}$ (90.2 kDa), T3$_{::myc}$ (49 kDa), T4$_{::myc}$ (56.3 kDa) and T5$_{::myc}$ (38.4 kDa) in endogenously tagged TFK1$_{::HA}$ PCF cells, using anti-myc antibody. Anti-enolase was used as loading control. (B) Immunofluorescence on whole cells with labeling of TFK1::myc (red) in non-induced (a) and induced cells (b), and (c-e) immunofluorescence on detergent extracted induced cells of truncations (T1::myc, T3::myc, and T5::myc) (red) after 24 h of induction of expression in endogenously tagged TFK1::HA background (green) PCF cells Scale bars: 5 µm, insets 1 µm.

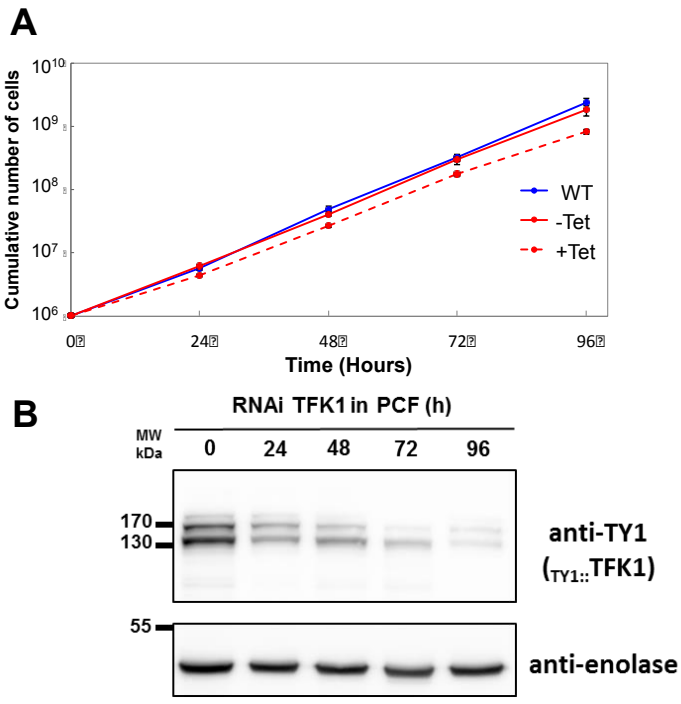

Fig. S6. TFK1 is not essential in PCF

(A) Growth curves of WT cells (blue line), non-induced cells (-Tet, red line) and tetracycline induced cells (+Tet, dashed red line) for TFK1 RNAi knockdown. (B) Western blot analysis of TFK1 protein level in endogenously tagged $_{TY1::}$TFK1 PCF using both anti-TY1 antibody before induction and 24, 48, 72 and 96 h post induction of TFK1 RNAi knockdown. Anti-enolase was used as loading control.

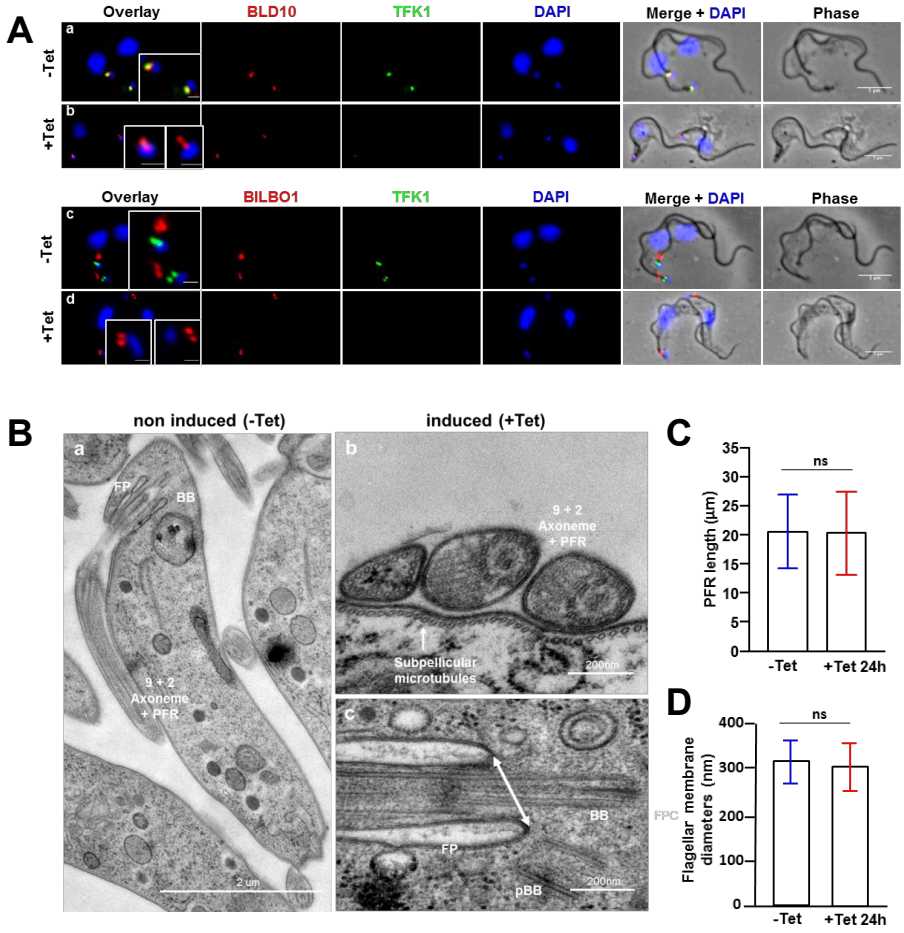

Fig. S7. Structural analysis of key organelles in TFK1 knockdown BSF cells

(A) Immunofluorescence on detergent-extracted BSF cells showing TFK1 (green) and BLD10 (BB marker, red) before (a, -Tet) and 24 h post induction of TFK1 RNAi knockdown (b, +Tet) and showing TFK1 (green) and BILBO1 (FPC marker, red) before (c, -Tet) and 24 h post induction (d, +Tet). Scale bar: 5 µm, inset 1 µm. (B) Transmission EM on thin sections of TFK1 RNAi non-induced (a) and induced 24 h (b, c) cells. PFR: paraflagellar rod, FP: flagellar pocket, FPC: flagellar pocket collar, BB: basal body, pBB: pro-BB. (C) Measurement of PFR length in BSF flagellar preparation labelled by anti-PFR antibody before (-Tet) and 24 h (+Tet) after TFK1 RNAi knockdown. (D) Measurement of the diameter of transition fibre structure from transmission EM images of longitudinal sections, by measuring the distance between the two sides of the flagellar pocket at the base of the flagellum (indicated by a white double-arrow on Bc) on non-induced and 24h-induced TFK1 RNAi knockdown BSF cells (n=19).

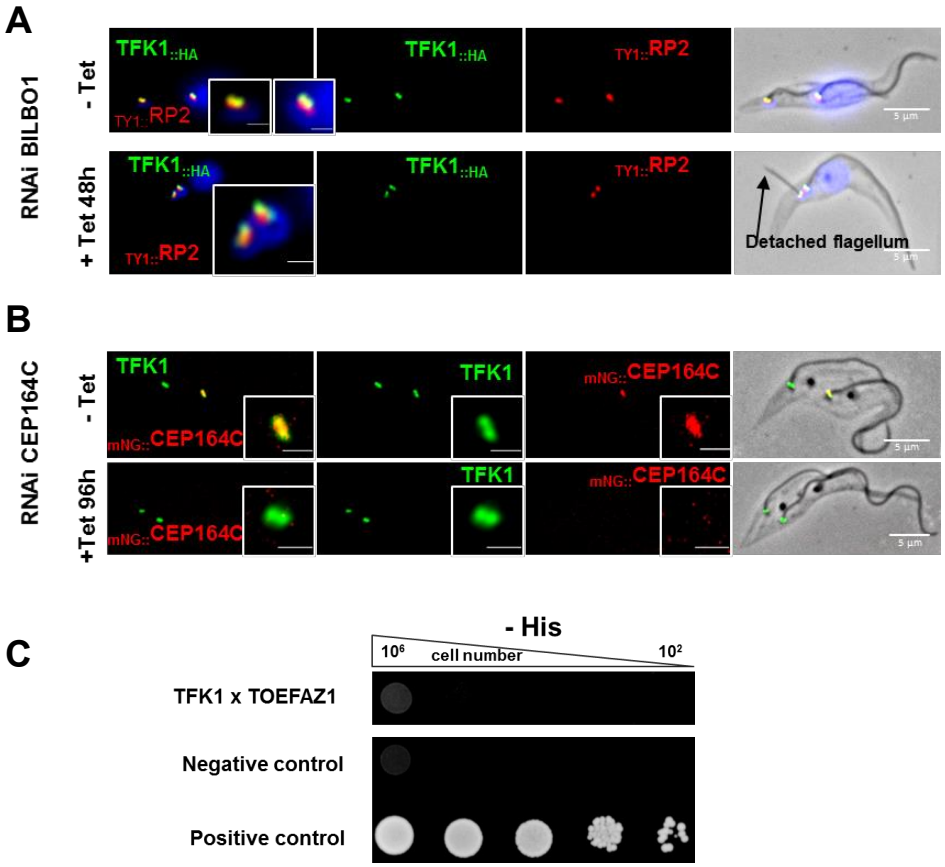

Fig. S8.TFK1 localization is not disturbed in BILBO1 RNAi or CEP164C RNAi knockdown cells and TFK1 and does not interact directly with TOEFAZ1 in Y2H assays (A) Immunofluorescence on detergent-extracted PCF cells showing the localization of TFK1$_{::HA}$ (green, anti-HA antibody) and $_{TY1::}$RP2 (red, anti-TY1 antibody) before (-Tet) and 48 h (+Tet 48h) after BILBO1 RNAi induction. (B) Immunofluorescence labelling of detergent-extracted PCF cells showing the localization of TFK1 (green, anti-TFK1) and $_{mNeonGreen::}$CEP164C (red, direct fluorescence) before (-Tet) and 96 h (+Tet 96h) after CEP164C RNAi induction. Scale bars: 5 µm, inset 1 µm. (C) Y2H interaction assay on – Histidine selective medium (-His) of TFK1 with TOEFAZ1/CIF1. Negative control: Lamin and T-antigen interaction, positive control: p53 and T-antigen interaction.

Table S1. Measurements of TFK1 immunogold labelling.

This table shows the measurements of the distance (indicated by the white double-arrow in Fig. 3C) from the center of the basal body to the gold labeling from transversal section iEM images (n=28). s.d: standard deviation.

Measurements of distance of TFK1 immunogold labelling on transversal section		
	Immunogold dot	Distance (nm)
micrograph n°21	1	160.8
	2	158.3
	3	172.8
	4	168.3
	5	160.6
micrograph n° 25	1	169.1
	2	163.4
	3	163.5
	4	178.5
	5	172.5
	6	166.2
	7	148.9
	8	163.4
micrograph n°6	1	221.7
	2	224.0
	3	180.5
	4	183.8
micrograph n°10	1	204.1
	2	204.2
	3	204.9
micrograph n°9	1	127.9
	2	141.3
	3	140.1
micrograph n°11	1	171.6
	2	187.1
	3	210.0
micrograph n°22	1	123.0
	2	154.0
	Mean (mn)	**172.3**
	s.d. (mn)	**25.9**